NASA TECHNICAL NOTE

NASA TN D-4015

NASA TN D-4015

EXPERIMENTAL AND ANALYTICAL STUDY OF THE TRANSIENT SOLIDIFICATION OF A WARM LIQUID FLOWING OVER A CHILLED FLAT PLATE

by Joseph M. Savino and Robert Siegel

Lewis Research Center
Cleveland, Ohio

NATIONAL AERONAUTICS AND SPACE ADMINISTRATION • WASHINGTON, D. C. • JUNE 1967

NASA TN D-4015

EXPERIMENTAL AND ANALYTICAL STUDY OF THE TRANSIENT SOLIDIFICATION OF A WARM LIQUID FLOWING OVER A CHILLED FLAT PLATE

By Joseph M. Savino and Robert Siegel

Lewis Research Center
Cleveland, Ohio

NATIONAL AERONAUTICS AND SPACE ADMINISTRATION

For sale by the Clearinghouse for Federal Scientific and Technical Information
Springfield, Virginia 22151 – CFSTI price $3.00

CONTENTS

EXPERIMENTAL AND ANALYTICAL STUDY OF THE TRANSIENT SOLIDIFICATION OF A WARM LIQUID FLOWING OVER A CHILLED FLAT PLATE

by Joseph M. Savino and Robert Siegel

Lewis Research Center

SUMMARY

Analytical predictions and experimental data are provided for the transient growth of a frozen layer that forms when a warm liquid flows over one side of a chilled flat plate. The plate is cooled to a temperature below the freezing point of the liquid by a coolant flowing along the other side of the plate. This could be encountered, for example, in a heat exchanger where water is being cooled by a cryogenic fluid. Three analytical procedures are employed and compared for accuracy and convenience in application. One is an iterative technique that yielded three closed-form solutions, each successive solution being a more accurate higher order approximation. Numerical results from the third approximation are presented graphically in sufficient detail so that rapid estimates of frozen layer growth can be made. In the experiment, water flowed over one side of a thin Inconel plate while the other side of the plate was cooled by flowing chilled alcohol. Transient ice growth was initiated by a sudden increase of the alcohol flow. The ice thickness and the plate surface temperatures were measured throughout the transient growth period and compared favorably with theoretically predicted values.

INTRODUCTION

This report is concerned with the transient solidification of a warm flowing liquid that is in contact with a chilled plane wall. The wall is cooled below the freezing point of the warm liquid by a coolant flowing on the opposite side. As the frozen layer grows on the surface, the warm liquid is continually supplying convective heat to the liquid - frozen layer interface. This convective heat combines with the latent heat released at the interface and is transferred through the frozen layer and wall into the coolant. This type of solidification problem arises in important and familiar applications, such as continuous casting of metals and freezing of rivers. The application that motivated the present study

is concerned with a number of advanced propulsion devices that utilize liquid - liquid heat exchangers in which the coolant is at a temperature below the freezing point of the warm liquid. One example is a water-to-liquid-hydrogen heat exchanger for possible application in a nuclear rocket engine. If the temperature or flow rate of the warm liquid is low enough, a frozen layer will form on the exchanger walls. Such an exchanger can operate satisfactorily if the frozen layer is not thick enough to severely restrict the flow passages. The prevention of serious blockage due to excessive solidification requires an understanding of the transient formation of the solid layer on the exchanger walls.

A review of the literature was made to uncover what information was available on solidification or melting problems with a convective boundary condition at the moving interface. Little analytical work was found for this type of boundary condition. For other types of boundary conditions, however, there were numerous mathematical studies as evidenced for example by references 1 to 5. Relatively few experimental studies were found, and of these none were for forced flow of the liquid over the moving interface. Some of the analytical studies are now reviewed since they form a foundation for the present analysis.

There are two reasons motivating the considerable number of mathematical studies. The first is the practical importance of moving interface problems in applications such as thermal storage devices for space vehicles, the formation of polar ice, and the freezing and thawing of soil. The second is that the problems offer a challenge for mathematical study because the moving boundary introduces a nonlinearity into the mathematics. The nonlinearity considerably increases the difficulty of finding solutions. As a result, exact solutions for transient frozen layer thicknesses and the accompanying temperature distributions and heat flows are usually difficult to obtain. Exact analytical solutions have only been found for simple configurations with certain types of boundary conditions. This has led to the situation where, in some instances, physically unrealistic boundary conditions have been imposed to acquire a mathematical solution. Some exact solutions for conditions of practical importance are summarized by Carslaw and Jaeger (ref. 6). One of these, for example, is the solution by Neumann for freezing (or melting) of a stationary semi-infinite medium initially at constant temperature, such as freezing a lake or melting a thick metal piece without removing the molten material. The semi-infinite medium is being cooled (or heated) by maintaining the boundary at a constant temperature.

When an exact analytical solution cannot be found, numerical or approximate methods must be employed. Murray and Landis (ref. 7) devised a numerical finite difference technique and demonstrated it for the following sample problems:

(1) A semi-infinite medium initially at the fusion temperature is subject to a step reduction in temperature at its boundary

(2) A slab of molten material of finite thickness initially above the fusion temperature is solidified by having its boundaries suddenly become subcooled.

Cochran (ref. 8) developed a lumped-parameter method wherein all the heat capacity is lumped at the center of the body and applied the method to a slab, a cylinder, and a sphere. A heat-balance integral approach was demonstrated on a variety of freezing and melting problems by Goodman (ref. 9). The temperature distribution in the material was approximated by a second- or third-order polynomial to evaluate an integrated form of the conduction equation. Adams (ref. 10) employed an iterative technique to find the frozen layer thickness and heat transfer in plane-, cylindrical-, and spherical-shaped metal castings with and without accounting for the conduction into the mold. This method does not involve any approximations in principle and provides successively iterated solutions that should approach an exact solution. In some instances, only the first iteration was conveniently carried out in analytical form. Cullom, et al. (ref. 11) employed the Crank-Nicolson finite difference technique to solve the problem of solidification of a stationary liquid at the fusion temperature onto a round tube cooled from within.

As mentioned, experimental results relevant to the present study are quite limited. Thomas and Westwater (ref. 12) studied freezing and melting in a thermal-conductivity-type cell. The cell was heated at the top, cooled at the bottom, and insulated on the sides to provide a unidirectional heat flow by conduction only through the freezing liquid. The primary test substance was n-octadecane and, for all conditions, the solid-liquid interface was seen to be populated with microscopic peaks and valleys. The measured velocities of the solidification front were as much as 100 percent higher than theoretically predicted. Observations of melting and freezing of p-xylene and water revealed that these substances provided smooth interfaces in contrast to the crystalline interface found for n-octadecane.

Tests of freezing and melting of water in absence of forced flow were conducted by Boger (ref. 13). Water was contained in a chamber 2 inches high bounded on top and bottom by copper blocks. The temperatures of the blocks could be regulated to obtain freezing or melting at either the upper or lower block. For some tests, the temperature range of the water within the chamber was entirely between the freezing point and the density inversion temperature (4° C). With these conditions, tests were conducted with no buoyancy forces present, and the freezing front velocities were found to agree quite well with values predicted by using the numerical technique in reference 7. When free convection was present, it was necessary to modify the theory by introducing an effective thermal conductivity to account for the convective transport.

Some experiments for melting in the presence of free convection are given in references 14 and 15. Reference 14 studies the melting of ice cubes by free convection in a water bath. In reference 15, the lower end of a vertical cylinder of ice was melted from below in a one-dimensional fashion by free convection from heated water. Comparison with theory indicated that the ice front melted more slowly than analytically predicted.

Solidification inside a tube and channel in the presence of laminar forced convection

was studied both experimentally and analytically by Zerkle (ref. 16). The wall of a circular tube and a pair of opposite walls of a rectangular channel were cooled so that ice layers formed. Zerkle was primarily interesting in developing a model for predicting the steady-state heat transfer and pressure drop inside channels whose walls were coated with ice.

In analytical models, the interface is usually assumed to be smooth and at the equilibrium freezing temperature. The details of crystal structure and undercooling at the solid-liquid interface have been studied in a number of experiments (refs. 17 to 21). For ice, if the propagation is into supercooled liquid where the heat of fusion is being discharged into the liquid, the interface is covered by a lattice of protruding crystals. For the present experiments, the liquid is above the freezing temperature, and the heat of fusion is being withdrawn by conduction through the ice layer. For these conditions, a smooth ice layer would generally be expected. Some comments concerning the interface will be made later in the discussion of the present experiment.

The present investigation was undertaken because of the lack of both analytical and experimental information on the transient solidification in a flowing medium. The objectives were to devise an analytical method for predicting the transient thickness of the solidified layer and accompanying temperature variations when a flowing fluid freezes on a cold plate and to compare the analytical results with experimental findings.

The model chosen for the analytical study is a locally one-dimensional solidification of a liquid that flows over one side of a thin flat wall. The other side of the wall is being convectively cooled by a fluid that is at a temperature below the freezing point of the liquid. The wall on which the liquid solidifies is assumed to be sufficiently thin so that the heat flow needed to subcool the wall during the transient is negligible compared with the heat flow through the wall. The heat flow through the wall is comprised of the latent heat of fusion, the subcooling heat capacity of the frozen layer, and the convection from the warm liquid at the solidified interface.

Three analytical methods were employed. For two of these, the transient heat-conduction equation that governs the energy balance within the solidified layer was integrated in a general way to provide an expression for the time required to form a specified instantaneous frozen layer thickness. The general integrated equation is evaluated for the present problem by using a method of successive analytically iterated approximations and also by using an approximate temperature profile of the type proposed by Goodman (ref. 9). The iterative technique is applied in this study in a different manner than the way it was applied by Adams (ref. 10). By the present method, higher order solutions can be found, and an analytical expression very close to an exact solution is obtained. The third analytical method is one proposed by Goodman (ref. 9) in which a heat balance at the liquid - frozen-layer interface is used.

The methods from reference 9 yielded two solutions that had to be integrated numer-

ically. The iterative method yielded three closed-form analytical expressions by means of three successively improved iterations. All the solutions are compared with regard to accuracy and ease of application. One of the closed-form solutions is sufficiently simple that it can be readily evaluated, and it yields quite accurate solidification times for all ranges of the parameters. Another closed-form solution, of a more complex form, represents for all practical purposes the exact solution and is used to evaluate the final results of the analysis that are presented in graphical form.

In the present experiment, ice was formed on a thin Inconel plate. Water at a bulk temperature above the freezing point passed in forced flow over one side of the plate while the other side was cooled by flowing chilled alcohol. Transients were initiated by suddenly starting the alcohol flow. The transient variations of ice thickness and plate surface temperatures were measured and are compared with theoretical predictions.

ANALYSIS OF SOLIDIFYING LAYER

The analysis deals with a one-dimensional configuration, as shown in figure 1. This represents an idealization of what can be achieved experimentally. Although the present experiment is for an ice-water system, the analysis could apply to any fluid that behaves within a reasonable approximation according to the conditions assumed (e.g., constant properties, solid-liquid interface at the equilibrium freezing temperature).

As a prelude to the analysis, it is instructive to trace the solidification process qualitatively. Before the start of any transient, a warm liquid at a fixed temperature T_l flows over one side of a thin plane wall. The warm liquid provides a convective heat-transfer coefficient h_l that is assumed to remain constant throughout the entire transient period before and during solidification. A coolant at a fixed temperature T_c flows over the opposite side of the plate where it provides a constant convective heat-transfer coefficient h_c. The resulting steady heat conduction through the plate establishes a linear temperature profile within it. If no coolant is flowing, the plate is at the temperature T_l of the warm liquid.

A transient solidification process can then be initiated in a number of ways, such as reducing the temperature or flow rate of the warm liquid, introducing the coolant if it had not been flowing, or lowering T_c of the flowing coolant. These changes cause the wall to further cool until the surface on the side of the plate exposed to the warm liquid reaches the freezing temperature. At this time, since the specific heat of the wall is neglected as an analytical simplification, a linear temperature distribution exists in the plate, as shown by the dotted temperature profile in figure 1. Solidification is assumed to begin as soon as the plate surface reaches the freezing point; that is, any subcooling necessary to initiate nucleation is neglected.

As the solidified layer on the wall increases in thickness, heat is extracted from the boundary layer of the warm liquid and is transferred by convection to the liquid-solid interface. There, it combines with the latent heat released by the solidification process and and is conducted through both the frozen layer and cold wall to the wall surface in contact with the coolant, where it is convectively removed. In general, an additional amount of heat removal is needed to subcool the frozen layer, and this is also transferred to the coolant (the heat removal necessary to subcool the wall is neglected in the analysis in comparison with the other heat flows). The solid layer continues to grow until it achieves a steady-state thickness X_s.

In the analysis and experiment, the time τ required to grow any given layer thickness $X(\tau) < X_s$ is measured from the moment solidification begins, which is taken as $\tau = 0$. The properties of the wall and the solid layer are assumed to be independent of temperature.

Steady-State Thickness of Frozen Layer

In many solidification problems, the frozen layer never approaches a steady-state thickness; rather it continues to propagate with time into the liquid. When, however, the liquid flowing over the frozen layer is at a temperature above the freezing point, the frozen layer will achieve a steady-state thickness. This thickness will be used as a reference length in the later analyses of growing layers and hence will be separately derived here.

It is assumed that the liquid-solid interface at the boundary of the frozen layer is at the freezing temperature T_f. Taking heat flow as positive in the positive x-direction, the convected flux from the liquid to the liquid-solid interface is

$$-q = h_l (T_l - T_f) \equiv \text{constant}$$

Using the overall heat-transfer resistance between the liquid-solid interface and the coolant gives the relation

$$-q = h_l (T_l - T_f) \equiv \frac{T_f - T_c}{\frac{X_s}{k} + \frac{a}{k_w} + \frac{1}{h_c}}$$

This is solved for the steady-state thickness

$$X_s = \frac{k}{h_l}\frac{T_f - T_c}{T_l - T_f} - k\left(\frac{a}{k_w} + \frac{1}{h_c}\right) \tag{1}$$

For $X_s = 0$, equation (1) gives the relation between variables required to just avoid freezing. For example, solving for T_l gives

$$T_l\Big|_{X_s=0} = T_f + \frac{T_f - T_c}{h_l\left(\frac{a}{k_w} + \frac{1}{h_c}\right)} \tag{2}$$

In order to prevent freezing, the liquid temperature T_l must be equal to or greater than the value given by equation (2).

General Equations for Frozen Layer Growth and Temperature Distribution

The heat flow within the frozen layer is governed by the transient heat-conduction equation; since constant properties are assumed, this has the form

$$k\frac{\partial^2 T}{\partial x^2} = \rho c_p \frac{\partial T}{\partial \tau} \tag{3}$$

When equation (3) is integrated from any position x within the layer to the solid-liquid interface X, there results

$$k\frac{\partial T}{\partial x}\Big|_X - k\frac{\partial T}{\partial x}\Big|_x = \rho c_p \int_x^X \frac{\partial T}{\partial \tau}\,dx \tag{4}$$

At the interface, the heat conducted into the solidified layer is equal to that supplied by the latent heat of fusion and the convection from the flowing liquid; that is,

$$k\frac{\partial T}{\partial x}\Big|_X = \rho L\frac{dX}{d\tau} + h_l(T_l - T_f) \tag{5}$$

Equation (5) is substituted into equation (4) to yield

$$-k\left.\frac{\partial T}{\partial x}\right|_x = -\rho L\frac{dX}{d\tau} - h_l\,(T_l - T_f) + \rho c_p\int_x^X \frac{\partial T}{\partial \tau}\,dx \tag{6}$$

The term on the left of equation (6) is the heat flux crossing any position x at any time τ. The first two terms on the right are the latent and convective heat fluxes originating at the solid-liquid interface, while the last term is the heat being removed by subcooling the portion of the solidified layer between x and X. The integration of equation (6) from the wall (x = 0) to any position x results in an expression for the instantaneous temperature distribution

$$T(x,\tau) - T_2 = \frac{\rho L}{k}\frac{dX}{d\tau}x + \frac{h_l}{k}(T_l - T_f)x - \frac{\rho c_p}{k}\int_0^x\int_x^X \frac{\partial T}{\partial \tau}\,dx\,dx \tag{7}$$

To eliminate the variable T_2, which is a function of time, equation (6) is written at x = 0 to give the heat flow at the wall, and this is equated to the heat flow through the wall and into the coolant to provide the relation

$$q(x=0) = -\rho L\frac{dX}{d\tau} - h_l\,(T_l - T_f) + \rho c_p\int_0^X \frac{\partial T}{\partial \tau}\,dx$$

$$= -\frac{T_2 - T_c}{\frac{1}{h_c} + \frac{a}{k_w}} \tag{8}$$

Then equation (8) is solved for T_2 and is substituted in equation (7) to give

$$T(x,\tau) = T_c + \left(\frac{1}{h_c} + \frac{a}{k_w}\right)\left[\rho L\frac{dX}{d\tau} + h_l\,(T_l - T_f) - \rho c_p\int_0^X \frac{\partial T}{\partial \tau}\,dx\right] + \frac{\rho L}{k}\frac{dX}{d\tau}x + \frac{h_l}{k}(T_l - T_f)x$$

$$-\frac{\rho c_p}{k}\int_0^x\int_x^X \frac{\partial T}{\partial \tau}\,dx\,dx \tag{9}$$

Equation (9) is placed in dimensionless form by letting

$$x' = \frac{x}{X_s}$$

$$X' = \frac{X}{X_s}$$

$$\tau' = \frac{h_l \left(T_l - T_f\right)\tau}{\rho L X_s}$$

$$T' = \frac{T - T_f}{T_c - T_f}$$

and using equation (1) in the form $(X_s h_l / k)\left[(T_l - T_f)/(T_f - T_c)\right] = R/(1 + R)$ to give

$$1 - T' = \frac{1 + Rx'}{1 + R}\left(\frac{dX'}{d\tau'} + 1\right) + \frac{RS}{1 + R}\left(\frac{1}{R}\int_0^{X'} \frac{\partial T'}{\partial \tau'}\, dx' + \int_0^{x'} \int_{x'}^{X'} \frac{\partial T'}{\partial \tau'}\, dx'\, dx'\right) \tag{10}$$

Because of the nondimensionalization, it is noted that two parameters, $S \equiv c_p(T_f - T_c)/L$ and $R \equiv (X_s/k)\Big/\left[(1/h_c) + (a/k_w)\right]$, have appeared. The subcooling parameter S is the ratio to the latent heat L of the maximum internal energy that could be removed if a unit mass of the solidified material were subcooled from the freezing temperature to the lowest temperature in the system T_c. This is not, however, a measure of the subcooling that actually occurs during the freezing process, since the entire solidified material does not reach this low temperature. The parameter R is a ratio of heat flow resistances. The X_s/k is the resistance offered by the steady-state thickness of the frozen layer, while $(1/h_c) + (a/k_w)$ is the combined resistance offered by the wall and the convective coefficient on the coolant side of the wall.

By applying the rules for differentiating under an integral, the integral terms of equation (10) can be transformed so that the derivative is taken outside the integral signs and equation (10) becomes

$$T' = 1 - \frac{1 + Rx'}{1 + R}\left(\frac{dX'}{d\tau'} + 1\right) - \frac{RS}{1 + R}\,\frac{\partial}{\partial \tau'}\left(\frac{1}{R}\int_0^{X'} T'\, dx' + \int_0^{x'} \int_{x'}^{X'} T'\, dx'\, dx'\right) \tag{11}$$

By reversing the order of integration, the double integral in equation (11) can be transformed into equivalent single integrals. This is accomplished by first writing the double integral in terms of dummy variables of integration η and β as follows:

$$\int_0^{x'} \int_{x'}^{X'} T'(x', X')dx'\ dx' \equiv \int_0^{x'} \int_{\eta}^{X'} T'(\beta, X')d\beta\ d\eta$$

where X' is treated as a constant. Reversing the order of integration leads to

$$\int_0^{x'} \int_{\eta}^{X'} T'(\beta, X')d\beta\ d\eta = \int_0^{x'} \int_0^{\beta} T'(\beta, X')d\eta\ d\beta + \int_{x'}^{X'} \int_0^{x'} T'(\beta, X')d\eta\ d\beta$$

$$= \int_0^{x'} \beta T'(\beta, X')d\beta + \int_{x'}^{X'} x'T'(\beta, X')d\beta$$

so that

$$\int_0^{x'} \int_{x'}^{X'} T'(x', X')dx'\ dx' = \int_0^{x'} x'T'(x', X')dx' + x' \int_{x'}^{X'} T'(x', X')dx' \qquad (12)$$

Equation (11) then takes the form

$$T'(x', X') = 1 - \frac{1 + Rx'}{1 + R}\left(\frac{dX'}{d\tau'} + 1\right)$$

$$- \frac{RS}{1 + R} \frac{\partial}{\partial \tau'}\left(\frac{1}{R}\int_0^{X'} T'\ dx' + x' \int_{x'}^{X'} T'\ dx' + \int_0^{x'} x'T'\ dx'\right) \qquad (13)$$

For convenience, let

$$I(x', X') \equiv \frac{1}{R}\int_0^{X'} T'\ dx' + x' \int_{x'}^{X'} T'\ dx' + \int_0^{x'} x'T'\ dx'$$

and note that

$$\frac{\partial I}{\partial \tau'} = \frac{\partial I}{\partial X'} \frac{dX'}{d\tau'}$$

As a result, equation (13) takes the form

$$T' = 1 - \frac{1 + Rx'}{1 + R}\left(\frac{dX'}{d\tau'} + 1\right) - \frac{RS}{1 + R}\frac{\partial I}{\partial X'}\frac{dX'}{d\tau'} \tag{14}$$

When equation (14) is evaluated at the solid-liquid interface $x' = X'$, there results

$$1 = \frac{1 + RX'}{1 + R}\left(\frac{dX'}{d\tau'} + 1\right) + \frac{RS}{1 + R}\frac{dG(X')}{dX'}\frac{dX'}{d\tau'} \tag{15}$$

where

$$G(X') \equiv I(x' = X', X') = \frac{1}{R}\int_0^{X'} T'\, dx' + \int_0^{X'} x'T'\, dx'$$

Solving equation (15) for $dX'/d\tau'$ gives

$$\frac{dX'}{d\tau'} = \frac{R(1 - X')}{1 + RX' + RS\dfrac{dG}{dX'}} \tag{16}$$

Separating the variables and integrating yield

$$\tau' = \int_0^{X'} \frac{1 + RX'}{R(1 - X')}\, dX' + S\int_0^{X'} \frac{1}{1 - X'}\frac{dG}{dX'}\, dX' \tag{17}$$

When the first integral on the right is evaluated and second integral is integrated by parts, the final expression for $\tau' = \tau'(X')$ is

$$\tau' = \left[-X' - \frac{1 + R}{R}\ln(1 - X')\right] + S\left[\frac{G(X')}{1 - X'} - \int_0^{X'} \frac{G(X')}{(1 - X')^2}\, dX'\right] \tag{18}$$

This is the expression that will be used to compute the frozen layer thickness as a function of time. Since $G(X')$ contains the temperature distribution, this distribution is obtained from equation (14) and equation (16) is used to eliminate $dX'/d\tau'$. The final relation for the temperature distribution in the frozen layer becomes

$$T' = \frac{R(1 - x')}{1 + R} - \left(\frac{1 + Rx' + RS \dfrac{\partial I}{\partial X'}}{1 + R} \right) \left[\frac{R(1 - X')}{1 + RX' + RS \dfrac{dG}{dX'}} \right] \tag{19}$$

Equation (19) is an integral equation for the temperature $T'(x', X')$. To solve equation (18), equation (19) must first be solved so that the integrals that comprise G in equation (18) can be evaluated. Two methods for carrying this out are examined herein.

The first method, and ultimately the more accurate of the two, is an iterative technique whereby the integrals in I and G are evaluated by using temperature distributions that are obtained from successively better approximations of equation (19). It appears that this procedure will ultimately lead to an exact solution. In the second method, equation (19) is not used. Instead, the temperature distribution to be used in $G(X')$ of equation (18) is approximated by a second-order polynomial with coefficients that are evaluated using the physical conditions at the boundaries of the frozen layer. Since this approximate temperature profile does not arise from the energy equation, the second method cannot yield an exact solution. The two methods are outlined in the next sections.

Solution by Analytical Iterations (AI Method)

An iterative procedure is utilized by Adams (ref. 10) for some solidification problems; before the present method is discussed, a few comments are in order. When Adams' procedure was applied to the problem under study herein, the first iteration (second approximation) resulted in a cumbersome quadratic equation for $dX'/d\tau'$. After the quadratic equation was solved, a numerical integration was required to determine X' as a function of τ'. A second iteration would have been extremely difficult and was not attempted. Hence, an alternate approach was devised in which higher order iterations could be analytically obtained. These will now be presented.

A first-order approximation to the temperature distribution and growth times is conveniently found by neglecting the effect of heat capacity within the frozen layer. When the c_p becomes zero, the parameter $S = 0$, and equations (18) and (19) reduce to

$$\tau_I' = -X' - \frac{1 + R}{R} \ln(1 - X') \tag{20}$$

$$T_I' = \frac{R(X' - x')}{1 + RX'} = \frac{RX'}{1 + RX'} (1 - \xi) \tag{21}$$

A second approximation for T' and $\tau' = \tau'(X')$ was obtained by substituting equation (21) for T'_I in equations (18) and (19) while retaining the S terms. After the integrations in $I(x', X')$ and $G(X')$ are performed, the results can be simplified to

$$\tau'_{II} = \tau'_I - S\left\{\frac{RX'}{3(RX'+1)}\left[X' + \frac{R+2}{R(R+1)}\right] + \frac{3+3R+R^2}{3(1+R)^2}\ln(1-X') + \frac{\ln(RX'+1)}{3R(1+R)^2}\right\} \tag{22}$$

and

$$T'_{II} = \frac{R(1-X'\xi)}{1+R} - \left(\frac{1 + RX'\xi + RS\left.\frac{\partial I}{\partial X'}\right|_I}{1+R}\right)\left[\frac{R(1-X')}{1 + RX' + RS\left.\frac{dG}{dX'}\right|_I}\right] \tag{23}$$

where

$$\left.\frac{dG(X')}{dX'}\right|_I = \frac{R^2}{(1+RX')^2}\left(\frac{X'}{R^2} + \frac{X'^2}{R} + \frac{X'^3}{3}\right) \tag{24}$$

$$\left.\frac{\partial I}{\partial X'}\right|_I = \frac{R^2}{(1+RX')^2}\left[\frac{1}{R}\left(\frac{X'}{R} + \frac{X'^2}{2}\right) + \left(\frac{X'^2\xi}{R} + \frac{X'^3\xi}{2}\right) - \left(\frac{X'^2\xi^2}{2R} + \frac{X'^3\xi^3}{6}\right)\right] \tag{25}$$

When the procedure is repeated, that is, when equation (23) is substituted into equations (18) and (19), the third approximation results, which is the final approximation evaluated herein; that is,

$$\tau'_{III} = \tau'_I + S\left[\frac{G_{II}(X')}{1-X'} - \int_0^{X'} \frac{G_{II}(X')}{(1-X')^2}\,dX'\right] \tag{26}$$

$$T'_{III} = \frac{R(1-X'\xi)}{1+R} - \left(\frac{1 + RX'\xi + RS\left.\frac{\partial I}{\partial X'}\right|_{II}}{1+R}\right)\left[\frac{R(1-X')}{1 + RX' + RS\left.\frac{dG}{dX'}\right|_{II}}\right] \tag{27}$$

where

$$G_{II}(X') = \frac{X' + \frac{R-1}{2}X'^2 - \frac{RX'^3}{3}}{1+R} + \left(\left.\frac{dX'}{d\tau'}\right|_{II}\right)\left[\frac{-\frac{X'}{R} - X'^2 - \frac{RX'^3}{3}}{1+R}\right.$$

$$\left. - \frac{R^3 S}{(1+R)(1+RX')^2}\left(\frac{X'^2}{R^3} + \frac{4X'^3}{3R^2} + \frac{2X'^4}{3R} + \frac{2X'^5}{15}\right)\right] \qquad (28)$$

$$\left.\frac{\partial I}{\partial X'}(X', \xi)\right|_{II} = \frac{(1+RX'\xi)(1-X')}{1+R} + \left(\left.\frac{dX'}{d\tau'}\right|_{II}\right)\left\{-\frac{(1+RX')(1+RX'\xi)}{R(1+R)}\right.$$

$$+ \frac{R^3 S}{(1+R)(1+RX')^2}\left[\left(\frac{1+RX'\xi}{R}\right)\left(-\frac{2X'}{R^2} - \frac{5X'}{2R} - \frac{5X'^3}{6}\right)\right.$$

$$\left. + \left(\frac{1+RX'}{R}\right)\left(\frac{X'^2\xi^2}{2R} + \frac{X'^3\xi^3}{6}\right)\right]$$

$$- \frac{2R^4 S}{(1+R)(1+RX')^3}\left[\left(\frac{1+RX'\xi}{R}\right)\left(-\frac{X'^2}{R^2} - \frac{5X'^3}{6R} - \frac{5X'^4}{24}\right)\right.$$

$$\left. + \left(\frac{X'}{R} + \frac{X'^2}{2}\right)\left(\frac{X'^2\xi^2}{2R} + \frac{X'^3\xi^3}{6}\right) - \frac{X'^4\xi^4}{24R} - \frac{X'^5\xi^5}{120}\right]\right\}$$

$$+ \frac{d}{dX'}\left(\left.\frac{dX'}{d\tau'}\right|_{II}\right)\left\{-\frac{\left(X' + \frac{RX'^2}{2}\right)(1+RX'\xi)}{R(1+R)}\right.$$

$$+ \frac{X'^2\xi^2 + \frac{RX'^3\xi^3}{3}}{2(1+R)} + \frac{R^3 S}{(1+R)(1+RX')^2}\left[\left(\frac{1+RX'\xi}{R}\right)\left(-\frac{X'^2}{R^2} - \frac{5X'^3}{6R} - \frac{5X'^4}{24}\right)\right.$$

$$\left.\left. + \left(\frac{X'}{R} + \frac{X'^2}{2}\right)\left(\frac{X'^2\xi^2}{2R} + \frac{X'^3\xi^3}{6}\right) - \frac{X'^4\xi^4}{24R} - \frac{X'^5\xi^5}{120}\right]\right\} \qquad (29)$$

$$\left.\frac{dG(X')}{dX'}\right|_{II} = \frac{1 + (R - 1)X' - RX'^2}{1 + R} + \frac{d}{dX'}\left(\left.\frac{dX'}{d\tau'}\right|_{II}\right)\left[\frac{-\frac{X'}{R} - X'^2 - \frac{RX'^3}{3}}{1 + R}\right.$$

$$\left. - \frac{R^3S}{(1 + R)(1 + RX')^2}\left(\frac{X'^2}{R^3} + \frac{4}{3}\frac{X'^3}{R^2} + \frac{2X'^4}{3R} + \frac{2X'^5}{15}\right)\right]$$

$$+ \left(\left.\frac{dX'}{d\tau'}\right|_{II}\right)\left[\frac{-\frac{1}{R} - 2X' - RX'^2}{1 + R} - \frac{R^3S}{(1 + R)(1 + RX')^2}\left(\frac{2X'}{R^3} + \frac{4X'^2}{R^2} + \frac{8X'^3}{3R} + \frac{2X'^4}{3}\right)\right.$$

$$\left. + \frac{2R^4S}{(1 + R)(1 + RX')^3}\left(\frac{X'^2}{R^3} + \frac{4X'^3}{3R^2} + \frac{2X'^4}{3R} + \frac{2X'^5}{15}\right)\right] \tag{30}$$

$$\left.\frac{dX'}{d\tau'}\right|_{II} = \frac{R(1 - X')}{1 + RX' + RS\left.\frac{dG}{dX'}\right|_{I}} \tag{31a}$$

$$\frac{d}{dX'}\left(\left.\frac{dX'}{d\tau'}\right|_{II}\right) = \left[(1 + RX')^3 + R^3S\left(\frac{X'}{R^2} + \frac{X'^2}{R} + \frac{X'^3}{3}\right)\right]^{-2}\left\{R\left[(1 + RX')^3\right.\right.$$

$$\left. + R^3S\left(\frac{X'}{R^2} + \frac{X'^2}{R} + \frac{X'^3}{3}\right)\right]\left[2R(1 - X')(1 + RX') - (1 + RX')^2\right]$$

$$\left. - R(1 - X')(1 + RX')^2\left[3R(1 + RX')^2 + R^3S\left(\frac{1}{R^2} + \frac{2X'}{R} + X'^2\right)\right]\right\} \tag{31b}$$

No attempt was made to analytically evaluate the integral in equation (26), since there did not seem to be any advantage to doing so because of its algebraic complexity. Since the entire equation was to be evaluated on a digital computer, the integration was performed numerically.

It is obvious from the complexity of the temperature distribution equations (eqs. (27) to (31)) that a fourth analytically determined approximation would be almost impossible to carry out. As will be shown, a fourth approximate solution is unnecessary because the AI method converged rapidly with the first three approximate solutions.

Approximate Solution by the Prescribed Temperature Method (PT Method)

The basic expression (eq. (18)) that predicts the dimensionless growth times τ' for a layer of thickness X' contains integrals in the function G of the instantaneous temperature distributions in the frozen layer. Because the temperature distributions appear as integrands, the growth time τ' is not very sensitive to the exact shape of the distribution. Therefore, using a reasonable approximation for the temperature profile should result in fairly accurate predictions for $\tau' = \tau'(X')$. This idea was first applied to problems of freezing and melting by Goodman (ref. 9).

For the problem being treated in this report, the temperature profile within the frozen layer is now approximated by a second-order polynomial of the form

$$T' = A(X' - x') + B(X' - x')^2 \tag{32}$$

Equation (32) already satisfies the boundary condition that the temperature should be equal to T_f at the liquid-solid interface. Two additional boundary conditions are used to evaluate A and B. The boundary condition at the wall is that the following heat balance be satisfied:

$$k \left.\frac{\partial T}{\partial x}\right|_{x=0} = \frac{T_2 - T_c}{\frac{1}{h_c} + \frac{a}{k_w}}$$

which has the dimensionless form

$$\left.\frac{\partial T'}{\partial x'}\right|_{x'=0} = R\left[T'(x' = 0) - 1\right] \tag{33}$$

Using equation (32) in equation (33) provides the condition

$$-A - 2X'B = R(AX' + BX'^2 - 1) \tag{34}$$

The second boundary condition is at the liquid-solid interface and is given by equation (5). Equation (5) is modified in order to express it entirely in terms of T, without $dX/d\tau$, by using the following relation that can be written for any location in the frozen layer:

$$dT = \left.\frac{\partial T}{\partial x}\right|_{\tau} dx + \left.\frac{\partial T}{\partial \tau}\right|_{x} d\tau$$

At the instant the interface moves through position x, $x = X$, $dx/d\tau$ becomes $dX/d\tau$, and the derivative $dT/d\tau = 0$ since the interface is always at T_f. Then,

$$\left.\frac{\partial T}{\partial x}\right|_{\substack{\text{at interface} \\ \text{at given time}}} \frac{dX}{d\tau} = -\left.\frac{\partial T}{\partial \tau}\right|_{\substack{\text{at fixed x as} \\ \text{interface moves} \\ \text{across that x}}} \tag{35}$$

This is used to eliminate $dX/d\tau$ from equation (5), so that

$$\left.\frac{\partial T}{\partial x}\right|_{X} = -\frac{\rho L}{k} \frac{\left.\frac{\partial T}{\partial \tau}\right|_{X}}{\left.\frac{\partial T}{\partial x}\right|_{X}} + \frac{h_l}{k}(T_l - T_f)$$

If the relation $\partial T/\partial \tau = (k/\rho c_p)(\partial^2 T/\partial x^2)$ from the conduction equation is used, this boundary condition can be rearranged into the form

$$\left(\left.\frac{\partial T}{\partial x}\right|_{X}\right)^2 = -\frac{L}{c_p}\left.\frac{\partial^2 T}{\partial x^2}\right|_{X} + \frac{h_l}{k}(T_l - T_f)\left.\frac{\partial T}{\partial x}\right|_{X}$$

In dimensionless form, it becomes

$$\left(\left.\frac{\partial T'}{\partial x'}\right|_{X'}\right)^2 = \frac{1}{S}\left.\frac{\partial^2 T'}{\partial x'^2}\right|_{X'} - \frac{R}{1+R}\left.\frac{\partial T'}{\partial x'}\right|_{X'} \tag{36}$$

The temperature profile (eq. (32)) is substituted into equation (36), and the result is rearranged into

$$B = \frac{S}{2}\left(A^2 - \frac{AR}{1+R}\right) \tag{37}$$

which gives B when A is known. Equations (34) and (37) are solved simultaneously to yield A; that is,

$$A = \frac{R}{2(1+R)} - \frac{1+RX'}{S(2X'+RX'^2)} + \left\{\left[-\frac{R}{2(1+R)} + \frac{1+RX'}{S(2X'+RX'^2)}\right]^2 + \frac{2}{S(2X'+RX'^2)}\right\}^{1/2} \tag{38}$$

The coefficient A is the root of a quadratic equation, and the positive sign in front of the square root was chosen so that A would approach the proper limit as steady state is achieved. The limit is found by realizing that the steady-state temperature profile in the frozen layer must be linear; hence, from equation (32), $B(X' \to 1) = 0$. Then, from equation (37), $A(X' \to 1) = R/(1+R)$, which is also the limit of equation (38).

Equations (37) and (38) give A and B as explicit functions of X' and, hence, the temperature distribution (eq. (32)) is given as a function of X' and x'. The temperature distribution is then used to evaluate the integrals in equation (18).

The quantity G(X') is

$$G(X') = \frac{1}{R}\left(\frac{A}{2}X'^2 + \frac{B}{3}X'^3\right) + \frac{AX'^3}{6} + \frac{BX'^4}{12} \tag{39}$$

while the quantity

$$\int_0^{X'} \frac{G(X')}{(1-X')^2}\,dX' \tag{40}$$

has to be integrated numerically because the A and B contained in G are very complicated functions of X'. Equation (18) is then evaluated to give the time required to form a thickness of frozen layer $\tau' = \tau'(X')$ for any values of the parameters R and S.

With A and B known as a function of X' and, hence, as a function of τ', the temperature profile in the frozen layer can be evaluated at any time during the layer growth from equation (32), which can also be placed in the form

$$T' = AX'(1-\xi) + BX'^2(1-\xi)^2 \tag{41}$$

Determination of Frozen Layer Growth by Integrating Heat Balance at Liquid-Solid Interface (IF Method)

This alternate approach suggested by Goodman (ref. 9) begins with the interface condition given by equation (35):

$$\frac{dX}{d\tau} = -\frac{\left.\frac{\partial T}{\partial \tau}\right|_X}{\left.\frac{\partial T}{\partial x}\right|_X} = -\left.\frac{\frac{k}{\rho c_p}\frac{\partial^2 T}{\partial x^2}}{\frac{\partial T}{\partial x}}\right|_X$$

This has the dimensionless form

$$\frac{dX'}{d\tau'} = -\frac{1+R}{RS}\left.\frac{\frac{\partial^2 T'}{\partial x'^2}}{\frac{\partial T'}{\partial x'}}\right|_{X'} \tag{42}$$

The approximate temperature profile (eq. (32)) is used to evaluate the derivatives at the interface to give

$$\frac{dX'}{d\tau'} = \frac{1+R}{RS}\frac{2B}{A}$$

The quantity B is eliminated by using equation (37), and the variables are then separated. The result is integrated to yield

$$\tau' = \int_0^{X'} \frac{dX'}{A\frac{1+R}{R} - 1} \tag{43}$$

This was integrated numerically for various R and S using A as a function of X' from equation (38). As in the previous method, the temperature distribution is found from equation (41) with B obtained from equation (37).

Comparison of Solutions

Figure 2 shows the growth of the solidified layer for a few values of the parameters R and S as predicted by four different equations presented in the analysis. Included are results for the case in which the subcooling in the frozen layer is neglected (S = 0) as computed from equation (20). First, the lower set of curves, where R = 0.01, is considered. In the limit, when heat capacity is neglected (S = 0), all the solutions obtained from equation (18) are in agreement by definition with that given by equation (20). When S is increased to a maximum practical value of 3, all the solution methods are in agreement and fall away only slightly from the S = 0 curve.

The upper set of curves in figure 2 is for R = 100, and results are shown for the complete range of S values. The curves for S = 3 represent the extreme case of a large heat-capacity effect and this, coupled with the large R value, provides the maximum deviation between the calculation methods. One of the most significant findings is the very close agreement between the second and third analytical iterations (curves AI_{II} and AI_{III}). This agreement indicates that the third iteration has converged very close to the exact solution, a fact that will be further demonstrated by the temperature distributions in figure 3. Hence, for practical purposes, the third iteration can be regarded as the correct solution. The method using a prescribed temperature profile (PT curves) is in very good agreement with the analytical iterations and, hence, the prescribed temperature method can also be used with good accuracy for the present problem. The interface method (IF curves) deviates somewhat from the other methods but, at a given τ', it still provides X' values within 5 percent of the correct solution. The reason for this deviation stems from the fact that the growth times are related to the first and second partial derivatives of the temperature at the interface (eq. (42)). For the IF method, these derivatives are obtained from the approximate temperature profile (eq. (32)) rather than from a solution of the energy equation as in the AI method.

Temperature Distribution Within Freezing Layer

A few temperature distributions within the freezing layer are shown in figure 3. The dimensionless temperature is shown as a function of position within the layer for four different dimensionless layer thicknesses. An interesting characteristic is that all the temperature profiles are fairly close to being linear. The heat convected by the warm liquid to the interface, combined with the latent heat of fusion that also arises at the interface, is conducted through the frozen layer and tends to establish a linear temperature profile. The heat capacity of the layer, however, tends to produce a curved profile. The fact that most of the temperature profiles are nearly linear suggests that the subcooling energy is

small compared with the convective and latent heats at the frozen layer interface. When heat capacity is neglected (S = 0), the temperature distribution is linear.

Figure 3(a) shows the temperature distributions as compared by various methods for large values of both R and S. The rapid convergence of the successive analytical iteration solutions (AI) is demonstrated. The difference between the temperature distributions for the second and third iterations is very small. If a fourth approximation were evaluated, it appears that it would be indistinguishable from the third approximation and would have an insignificant effect on the frozen layer growth curves in figure 2. The profiles evaluated from the PT and the IF methods are not too far removed from the AI profiles. Figures 3(b) and (c) show how the agreement of all the methods is improved as either S or R is made smaller.

Solidification Times as Function of R and S Parameters

While all the solutions agree well with the third AI, which is taken to be the correct solution, they vary considerably in their form and difficulty of evaluation. The simplest solution is equation (20) for the S = 0 condition, but its range of application is restricted to small R values, as indicated by figure 2. The second AI (eq. (22)) is quite accurate for all ranges of R and S and has a form that can be easily and quickly evaluated even on a desk calculator if necessary. The third AI, PT, and IF solutions all require a digital computer for their evaluation. For these reasons, the second AI solution is the most convenient analytical form given here for use in engineering applications. The graphical results presented herein were evaluated from the third AI solution (eq. (26)).

In figure 4 is presented the dimensionless time τ' as a function of R with S as a parameter. Each group of curves gives the τ' required to form a given frozen layer thickness X'. This set of curves is used later for comparison with the experimental results. This can easily be done when there is specified a solidifying liquid and wall material, both having known properties, and the values of a, T_l, T_c, h_l, and h_c. With this information, the quantities R and S can be calculated. From figure 4, the τ' values can be found by simple interpolation for each X' shown. Then the relation between dimensional τ and X can be calculated from the definitions of τ' and X'.

Additional discussion on the general interpretation of the analytical results is given in reference 22.

EXPERIMENTAL INVESTIGATION

Apparatus

Flow circuits. - The test system shown in figure 5(a) consisted of two flow loops,

one for water and the other for chilled alcohol. Ordinary tap water was recirculated from a 50-gallon insulated storage tank. The thermal capacity of the large water volume maintained its temperature constant during a test. The water passed through a flowmeter and then a cotton filter to remove small particles that might clog the flow damping screens in the test section.

The alcohol was recirculated through insulated piping from a 50-gallon insulated tank. Within this tank was a smaller stainless-steel tank that contained a mixture of dry ice and alcohol. By adjusting the liquid level in the inner tank and thereby regulating the extent of the cold surface area, the temperature of the alcohol in the outer tank could be adjusted to the desired value for a test.

Test section. - The test section consisted primarily of two rectangular channels that were separated by a dividing wall. The important features are shown in figure 5(b). An Inconel plate, 4 inches long, $1\frac{1}{4}$ inches wide, and 3/16 inch thick, was embedded in a sheet of laminated thermoplastic of the same thickness. This sheet was clamped between two channels thereby forming the dividing wall between them (see section BB, fig. 5(b)). The test plate orientation was horizontal. The flow channel walls were made principally from 1-inch-thick clear plastic to provide insulation and to facilitate illumination of the ice layer that was formed on the Inconel plate. Both sides of the water flow channel adjacent to the Inconel plate contained $1\frac{1}{4}$-inch-thick optical glass windows to minimize distortion in the view of the ice layer. A piece of porous filter material and a series of damping screens were provided in the water flow channel to produce a uniform velocity profile. In early tests, it was found that if care was not taken to have the water velocity uniform, the ice layer developed grooves and ridges parallel to the flow direction so that the ice thickness was not uniform across the $1\frac{1}{4}$-inch width of the test plate. With damping screens installed, the ice layer was very flat in the transverse direction. The alcohol channel, which was not as high as the water channel, contained a piece of filter material followed by one damping screen. The uniformity of the alcohol velocity was not as critical as for the water because the alcohol was not in direct contact with the ice.

Instrumentation. - The most important measurements required in the experiment were (1) the transient and steady-state temperatures on both surfaces of the Inconel test plate, (2) the bulk temperatures of the water and alcohol flowing over the test plate, and (3) the ice layer thickness during its transient growth period and at steady state. The methods used for each of these measurements are now described in detail.

Test plate surface temperatures: The surface temperatures of the Inconel plate were measured by nine thermocouples on each surface (fig. 5(b)). The pair of 0.003-inch-diameter enameled copper-constantan wires forming each thermocouple was cemented side by side inside a surface groove 0.007 inch wide, 0.005 inch deep, and 0.75 inch long. A thermocouple junction was formed by soldering the wire ends to the plate at the end of the groove. Then the surface in the vicinity of the thermocouple junction and along

the lead groove was smoothed by removing the excess solder and cement with a very fine abrasive. For convenience in handling, the thin lead wires were spliced (using a soldered joint) to thicker 0.020-inch-diameter wires of the same material. Originally, the splices were made in the region between the edge of the Inconel test plate and the outside surface of the viewing windows. Preliminary tests revealed that the temperature gradient along the length of the splices was causing errors in the surface temperature data because of extraneous voltages generated in the soldered splices. For the final test results, the splices were made in an isothermal region at room temperature several inches away from the outside surface of the test section.

The method of installing the thermocouples on the plate and the small wire diameter were chosen primarily to provide accurate surface temperature measurements during both the transient period and at steady state. The small size of the wire allowed the thermocouple to respond almost instantaneously to surface temperature changes, and minimized distortions of the local temperature distribution. The length-diameter ratio of the wires was made large enough to prevent errors arising from heat leakage from the junction through the leads.

Water and alcohol bulk temperatures: The bulk temperatures of the water and alcohol were measured with thermocouple probes at the inlets of their respective flow channels in the test section. The alcohol temperature was also checked with a thermocouple at the channel outlet. In the storage tanks, thermometers provided the temperature of each fluid as an approximate check on the values in the test section. The probes and thermometers were calibrated in a water-crushed ice mixture and at lower temperatures down to -60° F by comparison with a precision thermometer in a dewar of cold alcohol. All thermocouples could be read with either a precision hand potentiometer or a strip chart electronic recorder.

Ice-layer thickness measurements: Three basic methods were employed to measure the ice-layer thickness during the transient growth period and at steady state. These will be referred to as the (1) photographic (2) visual, and (3) temperature probe methods. These methods will be discussed in some detail for the benefit of those who may want to make similar measurements.

The photographic method that was used for some preliminary results employed a 70-millimeter camera equipped with a timer, automatic film advance, and strobe lights (fig. 6). With this equipment, a series of still photographs could be taken at predetermined time intervals throughout the growth period. The camera viewed the ice layer edgewise, as shown in figure 6. The photographs were enlarged to 8- by 10-inch size, and the ice thickness measured from them. This method proved to be of limited accuracy because of optical distortion effects, optical illusions, difficulties in obtaining exact camera alinement with the plane of the ice interface, and limited image magnification. It is worth mentioning that a 16-millimeter motion picture camera was tried but was unsatis-

factory because the pictures were too small to provide the necessary clarity. Generally, it was found easier and more accurate to obtain results by the visual method and with the temperature probe described next.

The visual method of measuring the local ice-layer thickness utilized a cathetometer and two film sheets with a grid printed on each (fig. 6). The grids consisted of a group of carefully spaced parallel horizontal reference lines with other lines at a 45° and 90° angle to those reference lines. The films were photographic reductions of a grid that was carefully ruled on a large piece of white poster board. The horizontal reference lines were 0.025 inch apart and were coded for easy identification of their position relative to a zero reference line. Short horizontal dashes spaced vertically 0.005 inch apart were made between the horizontal reference lines at 1/2-inch intervals along them. These grids were mounted on the outside of the optical glass windows and were positioned so that the zero reference line on each grid was in the plane of the top surface of the Inconel test plate. Hence, when the grids were viewed with a cathetometer telescope, two corresponding reference lines, one from each grid, were in the same plane at the correct height above the Inconel plate. To measure the ice thickness at any position along the layer length, the ice-water interface was sighted with the telescope and the interface position was read from the film grids.

In actual practice, two factors affect the accuracy with which the visual (and also the photographic) method can be used to measure ice-layer thicknesses. These were especially significant for measurements made during the transient growth period and for layers less than about 0.050 inch thick. The factors are the transparency of the ice layer and the optical distortion that resulted from the small density gradient in the thermal boundary layer above the ice-water interface. The 45° and 90° lines on the film grids were for the purpose of assessing the extent of any optical distortion that might be present.

The transparency of the layer made it difficult at times to detect the exact location of the ice-water interface. The interface definition was aided by judicially arranging the lighting and using a white background. It was found that the light positions had to be shifted for various tests. When the test conditions were changed, it was difficult to predict exactly how to adjust the photographic lighting to assure sharp interface definitions throughout the transient. This was a drawback in the photographic method since, after the test had been completed and the films developed, some of the images were sometimes lacking in clarity, and a complete set of transient data could not be measured. For this reason, the use of the cathetometer and film grids offered a distinct advantage over the use of photographs.

The optical distortion resulting from bending of light by the nonisothermal water displaced the image of the interface from its true position. To account for optical distortion and to have the means for checking and calibrating the visual thickness measurements, several devices were employed. A few reference lines at known heights above the Inconel

plate were scribed on the inside of the optical windows. Some metal pins of known heights were mounted on the plastic plate (that contained the Inconel inserts) downstream of the ice layer. These provided reference lengths inside the test section adjacent to the ice layer. A piece of stainless-steel rule with 1/64-inch divisions was also mounted vertically on the plastic plate to the rear of the Inconel test insert. For measurements of steady-state ice thicknesses, a micrometer head was mounted on top of the water channel, and a vertical traversing rod was extended down into the water stream. The rod position was above one of the thermocouple locations in the center region of the Inconel plate. After an ice layer had formed, the rod that had been initially withdrawn from the water stream could be moved down to touch the ice surface and the thickness could be measured with the micrometer. The rod had to be moved very quickly since it would distort the water flow pattern near the ice surface and would also conduct heat toward the interface; both these actions would tend to melt the ice away before the probe could touch it and the thickness reading could be obtained.

The optical distortion caused the grid lines that were viewed through the water to bend significantly in the vicinity of the ice-layer surface. To calibrate the system, a steady ice thickness was formed, and the cathetometer was sighted across the interface at the position along the layer where the micrometer probe was located. Thickness readings were then taken from the two grids and with the micrometer (a thermocouple probe described below was also used as a further check). It was generally found that the grid viewed through the water gave the thickness accurately while the grid on the front window read about 0.020 inch too large.

The third method used to measure the ice-layer thickness employed a thermocouple probe (fig. 6). The probe consisted of a butt-welded junction made from 0.003-inch Chromel constantan wires stretched between two needles mounted on a 0.100-inch-diameter shaft. The shaft extended through the top of the test section and was mounted in a micrometer head, so that the junction could be accurately positioned at any specified height above the test plate. By touching the ice layer with the junction, the layer thickness at that location could be determined. The section Test Procedure describes the measurement of transient ice thicknesses by use of the thermocouple probe.

The temperature probe was also used to check the readings of one of the Inconel plate surface thermocouples. This was done by lowering the probe junction to the surface; by design, the probe location was very close to one of the surface thermocouples.

Test Procedure

Obtaining transient data. - All the transients were initiated by a sudden increase of the alcohol flow. For most of the tests, a very small alcohol flow was initially present

to provide a small, very thin patch of ice on the plate. For a few tests, there was no initial alcohol flow and no ice patch; on starting the alcohol flow, the plate subcooled below the freezing point and ice suddenly flashed on.

The transient data was taken only in the central region of the plate length where the heat transfer was essentially one dimensional in conformity with the conditions of the analysis. The heat transfer through the ice layer and Inconel plate was two dimensional near both plate ends.

For a measurement of the instantaneous thickness, the cathetometer and grid films were first alined. The cathetometer was sighted at one of the thermocouple stations on the plate. The full alcohol flow was then turned on, and the moving ice interface was viewed with the telescope. The time when the ice interface moved past each grid line was noted, and the thickness was marked at that time on the temperature strip chart that recorded the upper and lower plate surface temperatures. Thus, the strip chart provided a record of the thickness and plate surface temperature variations with time.

An alternate means for measuring the transient thicknesses was by use of the thermocouple probe shown in figure 6. This method served as a check on the data obtained with the cathetometer. The use of the probe was possible for two reasons: (1) the thermocouple and its needle-like supports were sufficiently small so that no local distortions of the interface were observed when the thermocouple was placed in contact with it and (2) the interface temperature measured with the probe was always found to be between 31.7° and 32° F for transient and steady-state conditions. To measure the instantaneous thickness during the growth period, the probe junction was positioned 0.005 inch above the plate, and the probe temperature was monitored with a fast response recorder. As the ice layer grew, the probe temperature decreased and reached 32° F when the probe was contacted by the ice. The probe was then quickly raised 0.005 inch before it could freeze into the advancing layer. A step jump was produced on the recorder as the probe moved upward into the warm water stream. This procedure was repeated giving a series of steps on the recording chart at times corresponding to every 0.005 inch of the growth. The temperature probe method proved to be the best method for measuring the instantaneous thickness during the transient growth period. The measured thicknesses were accurate to within 0.001 inch; they were easy to obtain, and agreed well with those measured with the grids and telescope. Because the probe was divised relatively late in the duration of the experimental project, most of the data reported here were obtained with the cathetometer.

Calibration for heat leakage. - Although the sides and windows of the test section channels were about 1 inch thick, some heat leakage was expected from the room into the cold test plate and alcohol. Of even greater importance was the leakage from the warm water through the walls of the test section and into the side edges of the Inconel test plate. As a result, some of the heat being removed by the coolant originated from heat leakage

and not from the ice formation process. To determine a correction for heat leakage, the following procedure was utilized. A piece of polyurethane insulation was formed into the shape of an ice layer and glued to the surface of the Inconel test plate on the water side. In this way, the flow pattern in the water stream was comparable to that during a test with an ice layer, and the direct heat flow through the test plate was small. With this arrangement, the plate was found to be from 0° to 6° F above the alcohol temperature depending on the temperature levels of the alcohol and water; without heat leakage, the plate would be at the alcohol temperature. The heat leakage temperature difference between plate and alcohol was measured for various flow rates and various alcohol and water temperatures. As shown in appendix B, it is necessary to add this temperature difference to the measured alcohol temperature to obtain the alcohol temperature that is effective in the ice growing process.

Processing of Data

To compute the expected ice growth from theory for comparison with experiment, the parameters R and S must be known along with the quantities that relate dimensionless to actual thicknesses and times. Four important quantities are the thermal conductivities of the Inconel plate and the ice, and the heat-transfer coefficients on the water and alcohol sides.

Thermal conductivities. - Data for the Inconel plate thermal conductivity were obtained from references 23 and 24. For the range of the present tests, the plate temperatures varied from 32° F at the initiation of a transient to about -20° F at the end of a transient. For this temperature interval, the Inconel thermal conductivity k_w was taken as 7.8 Btu per hour per foot per $^{\circ}$F.

The thermal conductivity of the ice k was obtained from Ratcliffe (ref. 25) and was selected as 1.36 Btu per hour per foot per $^{\circ}$F. This was chosen as an average value for the temperature range 32° to -10° F ordinarily encountered in the present test series. Some comments regarding the ice conductivity are given later in connection with the test results.

Heat-transfer coefficients. - To compare the measured ice growth with the theoretically predicted values, the local convective heat-transfer coefficients on both the water and alcohol sides must be known for each flow rate. The coefficients must be known with good accuracy, since the predicted ice growth can be quite sensitive to them. The sensitivity arises from the form of equation (1), which shows that the steady-state thickness depends on the difference of two terms. As this difference becomes small compared with the magnitudes of the terms, the X_s value becomes increasingly sensitive to the h_l and h_c values.

A first attempt to determine h_l and h_c values was by using laminar boundary layer

theory for flow over a flat plate of uniform temperature. This always produced theoretical values about 25 percent below those measured experimentally by methods that are described next. The discrepancy could have resulted from a number of experimental factors such as imperfections in the uniformity of the experimental velocity profile, free convection, disturbances from the side walls of the flow channels, variable fluid properties, etc. An additional complication was that the cold alcohol absorbed air, and some bubbles would be released when the alcohol contacted the warm plate. This would increase the heat-transfer coefficient above the laminar value. For these reasons, it was thought best to experimentally calibrate the apparatus to determine the convective coefficients.

Two methods were used for experimentally obtaining the h_l and h_c values. One approach was to set the flow rates for both water and alcohol at values to be used in the transient ice formation tests but not have the alcohol cold enough to form ice. Then, the temperature drop through the Inconel plate was measured at the locations along the plate length where the ice growth would later be observed. The known plate conductivity was used to compute the heat flow through the plate, assuming one-dimensional heat flow, and the local heat-transfer coefficients on both sides of the plate were found by using the measured temperatures of the liquids. A shortcoming is that the h_l values determined by this method are for a nonuniform surface temperature condition, whereas the boundary condition with an ice layer is one of the uniform temperature. Consequently, the h_l values from a bare plate determination are only approximately applicable to conditions with an ice layer.

A second approach was to grow steady-state ice layers of various thicknesses by holding the flow rates constant and allowing the water or alcohol temperatures to be varied from one test to another. Both the ice layer and Inconel plate thicknesses could then be used as heatmeters to obtain local heat fluxes and the corresponding local convective coefficients. For a given water and alcohol flow rate, usually three different ice thicknesses were formed by, for example, holding the alcohol temperature constant and using three different water temperatures. The corresponding heat-transfer coefficients had about a 10-percent spread in values, and an average was taken to provide the coefficients characteristic of the fixed flow rates.

For the same flow rate, the deviations between the coefficients determined by the second method and those using a bare plate were a maximum of 12 percent. There was no criterion by which either of the two methods could be shown to be the best. Hence, for a given position on the plate, the local values determined from the two methods were averaged and used in the theoretical predictions. It should be noted that the effective coolant temperature as described in appendix B was the coolant temperature used for all processing of data for comparing experimental results with theory.

Use of data in theoretical predictions. - The theoretical predictions of X, T_1, and

T_2 involved the following important assumptions: (1) the h_l and h_c remain constant throughout the transient period, (2) the ice-liquid interface is always at 32° F, and (3) there is no contact resistance between the ice and the Inconel plate. Some discussion on the validity of these assumptions is given later. With a given set of test conditions h_l, h_c, T_l, and T_c, the quantities X_s, $X(\tau)$, $T_1(\tau)$, and $T_2(\tau)$ can be computed from the analysis. The theoretical steady-state ice thickness is computed from equation (1). The R and S values can then be found. Figure 4 is used with these R and S values to find the dimensionless time τ' corresponding to various X' values. The theoretical $X(\tau)$ variation is then found by using the definitions of the dimensionless variables to convert back to dimensional variables.

The calculation of the theoretical variations of $T_1(\tau)$ and $T_2(\tau)$ was simplified because, for the range of experimental conditions encountered in the present series of tests, the subcooling parameter S was always less than 0.25. For this small subcooling and because R was always of order unity, figure 3 shows that the temperature T_2 at the interface between the ice and plate was always very close to the values for the limiting solution when $S = 0$. For $S = 0$ and $x' = 0$, the temperature equation (eq. (19)) simplifies to

$$T' = \frac{T_2 - T_f}{T_c - T_f} = \frac{R}{1 + R} - \left(\frac{1}{1 + R}\right)\frac{R(1 - X')}{1 + RX'}$$

This yields the expression for T_2

$$T_2 = T_f + (T_c - T_f)\frac{RX'}{1 + RX'} \tag{44}$$

that was used for comparison with the experimental temperature trace at the ice-plate interface.

To calculate the theoretical Inconel-alcohol interface temperature $T_1(\tau)$, the heat conduction through the Inconel plate must be examined. One basic assumption made in the Analysis section was that the plate heat capacity was negligible. The validity of this assumption was examined for typical data by using equation (C5) developed in appendix C. The term

$$\frac{\rho_w c_{p,w} a}{6}\frac{\partial}{\partial \tau}(2T_1 + T_2)$$

in equation (C5) was evaluated by using the measured $T_1(\tau)$ and $T_2(\tau)$ shown in figures

8(a) and (b) and one of these results (for fig. 8(b)) is presented in figure 10. The maximum heat rate extracted to subcool the plate was less than 10 percent of the total heat flux through the plate. This maximum occurred early during the transient, and the subcooling contribution then diminished rapidly with time. The maximum correction to the calculated $T_1(\tau)$ was less than 1.5° F. For this reason, the values for $T_1(\tau)$ shown in the figures were calculated from a simplified form of equation (C5) in which the heat capacity term was neglected, that is,

$$h_c(T_1 - T_c) = \frac{k_w}{a}(T_2 - T_1) \tag{45a}$$

Therefore, solving for T_1,

$$T_1 = \frac{\frac{k_w}{a} T_2 + h_c T_c}{\frac{k_w}{a} + h_c} \tag{45b}$$

RESULTS AND DISCUSSION

Configuration of Steady-State Ice Layer

Before discussing the comparison of experimental data with theory, it is of interest to consider the shape of the steady-state ice layer that formed on the chilled plate. The shape is illustrated in figure 6(b) for the case where the entire plate is below the freezing temperature. The convective heat-transfer coefficient of the warm water is very high near the leading edge of the plate as is characteristic of flat-plate boundary-layer heat transfer. This causes the ice layer to have zero thickness very close to the leading edge. If the convective transfer from the warm water is high enough to raise a portion of the plate above freezing, then the leading edge of the ice layer is downstream from the plate leading edge. Since the convective heat transfer decreases with length along the plate, the ice thickness increases in the downstream direction. The ice-layer shape contour resembles that of a flow boundary layer (similar contours were obtained by Zerkle in ref. 16). The ice layer extended a short distance past the trailing edge of the plate, as shown in figure 5(b). The data in the present experiments were taken in the central region of the Inconel plate where the ice growth was very nearly one dimensional.

Transient Ice Growth and Surface Temperatures

Several typical sets of experimental data are now compared with theoretical predictions. The ice-layer thickness and surface temperatures of the Inconel plate are given as a function of time. Zero time is always taken at the moment when ice first appears at the location on the plate where the transient measurements are being taken.

The analysis assumes that, at zero time, the surface of the plate in contact with the water is at the freezing temperature and ice is beginning to form. In order to have the experimental conditions correspond as closely as possible with the assumptions of the analysis, it was necessary to provide a nucleus of ice on the plate by using a very low alcohol flow so that, when the full alcohol flow was started, the ice layer would immediately begin to spread over the plate. If this were not done, the plate would subcool as much as 12° F before ice would suddenly flash on the plate. The flashing of ice was accompanied by a step rise in plate temperature that was never large enough to raise the plate surface to 32° F. With a small patch of ice initially on the plate, the surface would still subcool about 1° F while the ice was spreading over the plate, but the initial condition duplicated within reason that assumed in the analysis. All the runs given herein, with one exception, are for the condition where a small ice nucleus was initially provided.

The results in figures 7(a) to (c) and 8(a) to (c) are for three test runs with approximately the same water and coolant temperatures and coolant heat-transfer coefficient, but with three different values of the heat-transfer coefficient in the flowing water. Figures 7(a) to (c) give the transient ice thickness, while figures 8(a) to (c) provides the corresponding variations of the plate surface temperatures. The h_l was varied by changing the water velocity, which had mean values of 0.18, 0.26, and 0.35 feet per second for figures 7(a) and 8(a), 7(b) and 8(b), and 7(c) and 8(c), respectively.

An inspection of figures 7(a) to (c) indicates a generally favorably agreement of experimental ice thickness with theory and, at any time, the theory would provide a suitable thickness estimate for engineering purposes. At this time, only the theoretical curve given by the solid line is being considered; this line was predicted as described in the Analysis. The dotted prediction was computed in part from the experimental data and is discussed later. All the experimental data exhibit the same characteristics when compared with theory (solid curve). The experimental growth starts a little more slowly than predicted and, when the thickness is about 15 percent of the steady-state value, the growth becomes more rapid than predicted. Sometimes, as in figure 7(b), the steady thickness is achieved much more abruptly than the gradual asymptotic approach that theory indicates. As expected, figure 7(a) with a low h_l provides a thicker steady-state layer than figure 7(c), which corresponds to a higher h_l and consequently has more heat convected to the ice-water interface.

Figures 8(a) to (c) show that the plate surface temperatures in all cases fall below the

predicted curves. The difference is generally of the order of 4° F. That the plate temperatures were colder than predicted from theory is consistent with the observed more rapid ice growth rates. Possible reasons for these discrepancies are discussed later.

Figures 7(d) and 8(d) show some data where the coolant temperature was not as low as that used for the previous figures. This provides a smaller steady-state ice thickness, which results in an R value about one-fourth of that in figures 7(a) and 8(a). The comparison with theory is of the same nature as in the previous figures, that is, more rapid experimental growth rates than theory with a tendency toward abruptly reaching a steady state, and experimental surface temperatures usually about 4° F below theory.

Figures 7(e) and (f) and 8(e) and (f) show two sets of data that were obtained for practically identical values of heat-transfer coefficients and liquid temperatures. The only difference is that the test in figures 7(e) and 8(e) was started without having an initial patch of ice on the surface. There is little difference in the transient ice growth, but there are some differences in the surface temperatures. This is shown in additional detail by the small inserts in figures 8(e) and (f).

The inserts show the measured temperature history for a short time before and after the ice forms at the measuring location. Figure 8(f) for the case with an initial ice patch shows that, after the full alcohol flow is started, the lower surface temperature T_1 decreases monotonically. The upper surface (temperature T_2) subcools to 30.5° F and then remains at that temperature for a few seconds. The temperature T_2 then decreases as the ice layer is growing in thickness. Figure 8(e), where there is no initial ice patch, exhibits a different behavior. The upper surface of the plate subcools to 20° F, and ice is then nucleated. The temperature T_2 quickly rises several degrees and then begins to drop off as the ice layer thickens. The lower surface of the test plate also experiences a small temperature rise at the time that the ice is nucleated. For the transient without an initial ice patch, the surface temperature throughout most of the transient remains about 2° to 4° F further below the theory than the temperatures obtained with an initial ice patch.

With regard to the sudden nucleation of ice without an initial ice patch, some interesting supplementary temperature data are shown in figure 9. The temperature-time traces shown in figure 9(a) were made by having the thermocouple probe within the thermal boundary layer of the water during a time span from shortly before the ice formed until after the probe became embedded in the ice layer. The measurements were made as follows: The cold alcohol flow was reduced so that no ice existed anywhere on the plate, and the probe was positioned at the desired location close to the plate surface. The full alcohol flow was suddenly introduced, and the probe output was continuously monitored on a strip chart recorder. Since only one thermocouple probe was used, the traces shown in figure 9(a) for various positions above the plate were taken in successive tests, but the temperature magnitudes can be compared because the tests were quite repro-

ducible. The time origin $\tau = 0$ in figure 9(a) was chosen to be at the local minimum of each trace since the abrupt temperature rise always occurred very close to the instant that the ice was observed to flash on the surface. Also shown is a cross plot of temperature against distance from the wall surface at $\tau = 0$ and $\tau = 2$ seconds (fig. 9(b)).

The results reveal the existence of a layer of subcooled water in contact with the wall prior to ice nucleation and a subsequent instantaneous temperature increase in the layer coincident with the sudden appearance of the ice layer. This temperature increase was probably caused by the fact that ice crystals are known to propagate quickly through subcooled water (ref. 19), and the heat of fusion that is released raises the mixture of water and ice crystals to the freezing temperature. A transient then follows in which some of the heat flow within the water boundary layer serves to adjust the temperature profile to the suddenly increased boundary temperature.

Discussion of Discrepancy Between Theory and Experiment

Various factors were investigated to try to determine why a deviation existed between theory and experiment and, in particular, why the plate temperatures were consistently below the theoretical values. These factors and some interesting supplemental results are now discussed.

Contact resistance between ice and plate. - A contact resistance between the ice and metal plate could account for part of the temperature discrepancy. Such a resistance was noted in the thermal conductivity experiments of Ratcliffe (ref. 25) when metal plates were bonded to the ends of thermal conductivity specimens. Several tests with the present apparatus were made to detect the presence of a contact resistance. Before forming any ice, the 0.003-inch-diameter thermocouple probe was positioned about 0.002 inch above the Inconel surface at a location along the plate close to one of the plate surface thermocouples. An ice layer was then formed, and the thermocouple became encased within the layer. For steady conditions when the layer had reached its final thickness, the probe temperature was within 0.7° of the surface temperature T_2. During the early period of ice layer growth, the probe temperature was 2° to 3° F higher than the instantaneous T_2. The fact that the probe was 0.002 inch above the plate would account for a substantial portion of this temperature difference; hence, the effect of contact resistance appears small enough to be neglected in the present study.

Temperature at moving and steady-state ice interface. - In the analysis, it was assumed that the moving ice interface was always at the equilibrium freezing temperature (32° F). Conceivably, for a very fast moving interface, the heat removal rate could be so large that the crystallization process would not be rapid enough to prevent the interface from becoming subcooled. No evidence of appreciable interface subcooling was detected

in the present experiments. Tests were conducted by setting the thermocouple probe at various distances from the cold surface and then growing an ice layer. The probe temperature was continuously monitored on a strip chart recorder and was always found to be within a few tenths of 1° F of 32° F at the instant that the interface was observed to come into contact with the probe. It is interesting to note that, as the ice contacted and grew around the probe, the temperature remained constant at about 31.7° F for 1/2 to $2\frac{1}{2}$ seconds depending on the cooling rate. This indicates that, adjoining the interface, there probably exists a thin region in which the crystallization process is occurring. The assumption in the analysis of an equilibrium temperature at the moving interface appears to be satisfactory.

The temperature of a stationary ice interface in flowing warm water was checked in two ways. By using a reduced alcohol flow, a small patch of ice was formed on the test plate such that the edge of the patch touched one of the surface thermocouples. For this condition, the thermocouple always indicated 32° F within the accuracy of the thermocouple calibration. A second approach was to touch the steady-state ice layer with the thermocouple probe. This approach always yielded a reading that was within $32 \pm 0.2^{\circ}$ F.

Transient variation in heat-transfer coefficients. - A possible cause of experimental deviations from theory is that the convective heat-transfer coefficients, assumed constant in the analysis, are somewhat variable during an experimental transient. As the ice layer grows, the temperature of the Inconel test plate decreases and, consequently, the average temperature decreases in the alcohol thermal boundary layer. This produces an increase in alcohol viscosity and a decrease in coolant heat-transfer coefficient as the transient proceeds.

An additional experimental complication was the absorption of air by the cold alcohol. In the early part of the transient when the Inconel plate was still relatively warm, the contact of the alcohol with it would cause some bubbles to be released, thereby producing turbulence. The bubble release would decrease as the transient proceeded and the plate temperature decreased. This would enhance the alcohol coefficient in the early portion of the transient.

On the water side, the ice layer growth produces a reduction in the flow cross section that is a maximum of 20 percent corresponding to the thickest ice layer tested. This would increase the water velocity and the convective coefficient during the transient. Both a higher alcohol-side coefficient and a lower water-side coefficient during the earlier portion of the transient would cause a relatively more rapid ice growth during this part of the transient.

Heat fluxes. - A further comparison of measured and predicted results was made by examining the heat fluxes through the ice layer and wall and into the coolant. These fluxes are exactly equal at steady-state conditions only. During the transient period, the heat rates required to subcool the ice and the wall are also present. The heat leaving the

ice layer and entering the wall includes the convective heat $h_l (T_l - T_f)$, the heat of fusion liberated at the ice-water interface, and the heat for subcooling the ice. Similarly, the energy transferred to the coolant $h_c(T_1 - T_c)$ consists of the heat entering the wall plus the energy to subcool the plate. When the subcooling of the ice and plate is small, which was true throughout most of the transient period, the instantaneous heat flux through each can be computed from the instantaneous temperatures inserted into the steady-state conduction equation.

Using this type of quasi-steady-state calculation, a typical set of heat fluxes was calculated from the experimental data given in figures 7(b) and 8(b). The fluxes are shown in figure 10 along with the theoretical curve. The data in other parts of figures 7 and 8 yielded similar heat flow curves. For the major portion of the growth period (following about the first 80 sec), the instantaneous heat flux through the wall agrees with the flux into the coolant as it should. These portions of the curves, however, are displaced to earlier times than the theory; this is consistent with a similar behavior for the surface temperatures and the more rapid observed ice growth. The explanation for this displacement is not known. For times earlier than about 80 seconds, the heat flow through the wall is larger than that to the coolant, indicating that possibly a larger h_c should have been used to compute q_c during the early portion of the transient. The larger h_c could have been caused by the air bubbles leaving the alcohol adjacent to the plate as mentioned earlier. The bubble release was larger during the early portion of the transient when the plate temperature was the highest.

The largest discrepancy in figure 10 is the computed heat flux through the ice, which is larger than the other heat fluxes, especially at early times. This indicates that perhaps the ice conductivity value used to compute q_i is too large. A smaller k would provide an extra heat flow resistance across the ice layer, which would account for the low surface temperatures measured but would not account for the more rapid experimental ice growth. There is some foundation for the belief that k would be low during early ice growth. Early during the transient when the ice growth was rapid, the layer contained some air bubbles, and the ice and its surface appeared to be diffuse. As the layer became thicker and the growth was slower, the ice was clear and its surface was very smooth and transparent. In the ice thermal conductivity tests of Powell (ref. 26), low conductivities were detected when ice was initially frozen on a plate. It was found necessary to apply heat to the plate to melt the ice adjacent to the plate and then refreeze it in order to obtain conductivities consistent with those normally quoted in the literature. Thus, it is suggested that the ice with the diffuse appearance has a different k than the clear ice.

Ice growth computed from measured surface temperature. - To provide an additional examination of the consistency of the experimental data, computations were carried out where the ice growth was computed using the measured surface temperature $T_2(\tau)$ as a

known boundary condition. This calculation eliminates the uncertainties involved in the Inconel plate conductivity and the alcohol heat-transfer coefficient and determines whether the observed ice growth is in accord with a theory using a variable surface temperature as the boundary condition. In the present computations, the ice heat capacity was neglected because the S values were small for the present experiments. The analytical expression used was obtained by evaluating equation (7) at $x = X$ and omitting the heat capacity integral on the right side. This gives, after rearrangement,

$$\frac{dX}{d\tau} = \frac{k}{\rho L X}\left[T_f - T_2(\tau)\right] - \frac{h_l}{\rho L}(T_l - T_f) \tag{46}$$

This equation was integrated numerically using the experimental T_2 variation. The results are shown as a dot-dashed line in figure 7. The agreement with the data is generally as good and sometimes a little better than the prediction using the coolant heat-transfer coefficient. The observed ice thickness at any time is always less than what would be expected from the recorded surface temperature variation. This indicates, as was pointed out previously, that, during part of the transient period, the ice conductivity may be lower than the conductivity values reported in the literature. It is evident that there are several factors in the experiment that could, in a combined way, account for the observed deviations from theory. To better understand the details of the freezing process, more detailed measurements would be desirable, possibly with a thermocouple rake to obtain the details of the temperature variations within the ice. The range of experimental operating conditions should also be extended, for example, to lower coolant temperatures.

CONCLUSIONS

Analysis

The goal of the analysis was to develop a means for predicting the transient growth of the frozen layer that forms when a flowing warm liquid is in contact with a cold flat plate that is convectively cooled on the opposite side. This goal was achieved by employing the following two basic approaches: (1) by integrating the transient conduction equation over the entire frozen layer thickness and (2) a heat balance at the frozen layer - liquid interface.

By use of a proper dimensionless layer thickness and time variable, the dimensionless frozen layer growth can be expressed as a function of two parameters. One parameter provides a measure of the maximum possible subcooling energy of the frozen layer as compared with the latent heat of fusion. The second parameter is the ratio of the heat

flow resistance of the steady-state layer to the combined resistance of the wall and convection coefficient on the coolant side.

The results of the analysis led to a number of conclusions. Two of the five solutions that were derived were the most convenient to use and the most precise. Both were successive iterative approximations that were analytically derived. One of these approximations was sufficiently simple that it could easily be evaluated on a desk calculator, while the other appeared to converge to the correct solution and was used to prepare the final graphical results. These results suggest that the analytical iterative technique developed herein is a rapidly converging means for solving nonlinear transient freezing problems.

There are two additional conclusions that can be drawn from the analytical results. The first is that the subcooling of a frozen layer during its formation slows the growth rate substantially for some conditions. This is particulary true of thick layers. The second is that the temperature profiles in the frozen layer were found to be almost linear at all times. This suggests that the energy required to subcool the frozen layer is much less than the combined convective and latent heat passing through the layer.

Experimental Study

In the experimental study, ice was formed on an Inconel plate cooled by flowing chilled alcohol. Measurements were made of the instantaneous ice-layer-thickness and plate surface temperatures throughout the transient growth period. The most significant findings are summarized as follows:

1. The experimental transient ice thicknesses any any time during the ice growth were generally within 15 percent of the theoretically predicted values. However, the following departures between theory and experiment were evident:

   a. The experimental ice growth was generally more rapid than predicted, and the steady-state frozen thickness was reached more abruptly than expected from the theoretical asymptotic approach to steady state.

   b. The measured temperatures on both surfaces of the Inconel test plate were about 4^{o} F below theoretical predictions throughout most of the transient.

2. Very little contact resistance was found at the interface where the ice was frozen onto the Inconel plate.

3. The surface of the ice for both growing and steady-state ice layers in flowing warm water was always found to be, within a fraction of a degree, at the equilibrium freezing temperature 32^{o} F.

4. If there is no ice initially on the metal plate, the plate will usually subcool, as much as 12^{o} F in some instances, before ice is nucleated. Ice will then rapidly flash over the entire plate. This is accompanied by a sudden increase in surface temperature,

but the surface temperature never rises to the freezing point. Following the initiation of ice in this manner, throughout most of the transient, the temperatures remained further below predicted values than the measurements taken with an initial ice patch.

5. During the early stages when the ice growth was rapid, the layer contained some air bubbles and the ice surface appeared diffuse. As growth became slower, the layer was very clear and the surface very smooth and transparent.

6. Care must be taken when making visual measurements of ice thicknesses in flowing warm water because of optical distortion near the ice interface.

7. A computation of instantaneous heat flow through the ice indicates that the ice conductivity during the early growth period may have been smaller than later in the transient. This is also indicated by the ice thickness variation computed from the measured surface temperature.

Lewis Research Center,
National Aeronautics and Space Administration,
Cleveland, Ohio, December 12, 1966,
129-01-09-02-22.

APPENDIX A

SYMBOLS

A	coefficient of linear term in approximate temperature profile
a	thickness of the wall on which frozen layer is forming
B	coefficient of quadratic term in approximate temperature profile
c_p	specific heat at constant pressure of solidified material
$c_{p,w}$	specific heat of wall on which frozen layer is forming
h	convective heat-transfer coefficient
k	thermal conductivity of solidified material
k_w	thermal conductivity of wall on which frozen layer is forming
L	latent heat of fusion for solidifying material
q	heat flow per unit area in the positive x direction
R	dimensionless thermal resistance parameter, $(X_s/k)/\left[(1/h_c) + (a/k_w)\right]$
S	dimensionless subcooling parameter, $c_p(T_f - T_c)/L$
T	temperature
T'	dimensionless temperature, $(T - T_f)/(T_c - T_f)$
T_c	coolant temperature (effective value for solidification)
$T_{c,m}$	measured (uncorrected for heat leakage) coolant temperature
v	fluid velocity
X	thickness of frozen layer
X'	dimensionless thickness of frozen layer, X/X_s
X_s	thickness of the frozen layer at steady state
x	position coordinate in frozen layer measured from wall
x'	dimensionless coordinate, x/X_s
y	position coordinate in wall measured from wall-coolant interface
ξ	dimensionless coordinate, x/X
ρ	density of solidified material
ρ_w	density of wall
τ	time
τ'	dimensionless time, $\tau h_l (T_l - T_f)/\rho L X_s$

Subscripts:

c	coolant
f	at freezing point
ins	insulated
l	liquid phase of solidifying substance

w	wall material
1	test plate surface in contact with coolant
2	interface of solidifying material and wall
I, II, III	successive iterative approximate solutions

APPENDIX B

CORRECTION ON COOLANT TEMPERATURE TO ACCOUNT FOR HEAT LEAKAGE

A cross section through the ice layer as shown in section B-B of figure 5(b) yields the configuration shown in figure 11. The heat flow q_1 goes through the ice and the Inconel plate and corresponds to the one-dimensional heat flow considered in the theory. The heat flow q_2 is a heat leakage, and it is assumed to leak through the edges of the plate and does not pass through the plate in the manner of q_1. This assumption was deduced from some experiments in which the upper surface of the plate was insulated. For this condition, the temperatures T_1 and T_2 were found to be close together and were both above $T_{c,m}$.

From equation (8), the heat flux at the ice-wall interface can be written as

$$-\rho L \frac{dX}{d\tau} - h_l (T_l - T_f) + \rho c_p \int_0^X \frac{\partial T}{\partial \tau} dx = -\frac{T_2 - T_1}{\frac{a}{k_w}} \tag{B1}$$

The heat flux from the plate to the coolant includes q_2 and is expressed by

$$\frac{T_2 - T_1}{\frac{a}{k_w}} + q_2 = h_c (T_1 - T_{c,m}) \tag{B2}$$

Equation (B2) is solved for T_1 and substituted into equation (B1). The result can then be placed in the form

$$-\rho L \frac{dX}{d\tau} - h_l (T_l - T_f) + \rho c_p \int_0^X \frac{\partial T}{\partial \tau} dx = -\frac{T_2 - \left(T_{c,m} + \frac{q_2}{h_c}\right)}{\frac{1}{h_c} + \frac{a}{k_w}} \tag{B3}$$

By comparing equation (B3) with equation (8), it is evident that the quantity $T_{c,m} + (q_2/h_c)$ is the effective coolant temperature when heat leakage is present. For the tests where the water side of the test plate is insulated, T_2 is equal to T_1 and equation (B2) reduces to

$$q_2 = h_c\left(T_1 - T_{c,m}\right)_{ins}$$

which provides an expression for q_2. Thus, the effective coolant temperature that should be used when comparing the experiment with the one-dimensional analysis is

$$T_c = T_{c,m} + \left(T_1 - T_{c,m}\right)_{ins} \tag{B4}$$

APPENDIX C

CORRECTION OF COMPUTED HEAT FLUX TO COOLANT TO ALLOW FOR HEAT CAPACITY OF PLANE WALL

For the wall on which the ice layer is growing (fig. 12), the heat-conduction equation is

$$k_w \frac{\partial^2 T_w}{\partial y^2} = \rho_w c_{p,w} \frac{\partial T_w}{\partial \tau} \tag{C1}$$

Integrating twice with respect to y yields

$$-k_w \left.\frac{\partial T_w}{\partial y}\right|_{y=0} = -\frac{k_w}{a}(T_2 - T_1) + \frac{\rho_w c_{p,w}}{a} \frac{\partial}{\partial \tau} \int_0^a \int_0^y T_w \, dy \, dy \tag{C2}$$

The term on the left is then expressed in terms of the convective heat-transfer coefficient between the coolant and wall,

$$h_c(T_1 - T_c) = \frac{k_w}{a}(T_2 - T_1) - \frac{\rho_w c_{p,w}}{a} \frac{\partial}{\partial \tau} \int_0^a \int_0^y T_w \, dy \, dy \tag{C3}$$

The double integral is the contribution from the specific heat term and is a correction for equation (45a). An approximate value for the double integral can be evaluated by using the following linear approximation for T_w:

$$T_w = T_1 + \frac{T_2 - T_1}{a} y \tag{C4}$$

After carrying out the integration, the heat flow to the coolant becomes

$$h_c(T_1 - T_c) = \frac{k_w}{a}(T_2 - T_1) - \frac{\rho_w c_{p,w} a}{6} \frac{\partial}{\partial \tau}(2T_1 + T_2) \tag{C5}$$

The importance of the heat capacity correction can be evaluated from the measured $T_1(\tau)$ and $T_2(\tau)$ where the derivative

$$\frac{\partial}{\partial \tau}\left[2T_1(\tau) + T_2(\tau)\right]$$

is evaluated by finite differences.

REFERENCES

1. Boley, Bruno A.: The Analysis of Problems of Heat Conduction and Melting. High Temperature Structures and Materials, A. M. Freudenthal, B. A. Boley, and H. Liebowitz, eds., Pergamon Press, Inc., 1964, pp. 260-315.

2. Kreith, F.; and Romie, F. E.: A Study of the Thermal Diffusion Equation with Boundary Conditions Corresponding to Solidification or Melting of Materials Initially at the Fusion Temperature. Phys. Soc. Proc., Sect. B, vol. 68, pt. 5, May 1955, pp. 277-291.

3. Hrycak, Peter: Problem of Solidification with Newton's Cooling at the Surface. A.I.Ch.E. J., vol. 9, no. 5, Sept. 1963, pp. 585-589.

4. Citron, Stephen J.: Heat Conduction in a Melting Slab. J. Aero/Space Sci., vol. 27, no. 3, Mar. 1960, pp. 219-228.

5. Muehlbauer, John C.; and Sunderland, J. Edward: Heat Conduction with Freezing or Melting. Appl. Mech. Rev., vol. 18, no. 12, Dec. 1965, pp. 951-959.

6. Carslaw, H. S.; and Jaeger, J. C.: Conduction of Heat in Solids. 2nd ed., Oxford at the Clarendon Press, 1959, pp. 282-296.

7. Murray, William D.; and Landis, Fred: Numerical and Machine Solutions of Transient Heat-Conduction Problems Involving Melting or Freezing. Pt. I - Method of Analysis and Sample Solutions. J. Heat Transfer, vol. 81, no. 2, May 1959, pp. 106-112.

8. Cochran, David L.: Rate of Solidification-Application and Extension of Theory. Tech. Rep. No. 24, Dept. of Mech. Eng., Stanford University, Apr. 1955.

9. Goodman, T. R.: The Heat-Balance Integral and Its Application to Problems Involving a Change of Phase. ASME Trans., vol. 80, no. 2, Feb. 1958, pp. 335-342.

10. Adams, C. M., Jr.: Thermal Considerations in Freezing. Liquid Metals and Solidification, Amer. Soc. for Metals, 1958, pp. 187-217.

11. Cullom, Richard R.; Diedrich, George; and Albers, Lynn U.: Analysis of Solidification in Thermal-Energy Storage Systems With Axisymmetric Heat-Transfer Solutions. NASA TN D-3763, 1966.

12. Thomas, L. J.; and Westwater, J. W.: Microscopic Study of Solid-Liquid Interfaces During Melting and Freezing. AICh.E Chem. Eng. Progr. Symp. Ser., vol. 59, no. 41, 1963, pp. 155-164.

13. Boger, David V.: The Effect of Buoyancy Forces on the Melting and Freezing Process. Ph.D. Thesis, Univ. of Illinois, 1965. (Also available in ASME Trans.,

J. Heat Transfer, vol. 89, Series C, no. 1, Feb. 1967, pp. 81-89 by D. V. Boger and J. W. Westwater.)

14. Filatkin, V.: Investigation of Heat Transfer During the Melting of Ice Under Free Flow Conditions. Kholodil'naya Tekh., vol. 37, no. 4, 1960, pp. 23-25.

15. Yen, Y. C.; Tien, C.; and Sander, G.: An Experimental Study of a Melting Problem with Natural Convection. Proceedings of the 3rd International Heat Transfer Conference, Chicago, ASME, AIChE, Aug. 1966, vol. IV, pp. 159-166.

16. Zerkle, Ronald D.: Laminar Flow Heat Transfer and Pressure Drop in Tubes with Liquid Solidification. Ph.D Thesis, Georgia Institute of Technology, Sept. 1964.

17. Hallett, J.: Crystal Growth and the Formation of Spikes in the Surface of Supercooled Water. J. Glaciology, vol. 3, 1960, pp. 698-705.

18. Harrison, J. D.; and Tiller, W. A.: Ice Interface Morphology and Texture Developed During Freezing. J. Appl. Physics, vol. 34, no. 11, Nov. 1963, pp. 3349-3355.

19. Hallett, J.: Experimental Studies of the Crystallization of Supercooled Water. J. Atmospheric Sci., vol. 21, no. 6, Nov. 1964, pp. 671-682.

20. Macklin, W. C.; and Ryan, B. F.: The Structure of Ice Grown in Bulk Supercooled Water. J. Atmospheric Sciences, vol. 22, no. 4, July 1965, pp. 452-459.

21. Hunt, J. D.; and Chilton, J. P.: An Experimental Investigation of the Undercooling at the Solid/Liquid Interface of the Lead-Tin Eutectic. Inst. Metals J., vol. 92, 1963-1964, pp. 21-25.

22. Siegel, R.; and Savino, J. M.: An Analysis of the Transient Solidification of a Flowing Warm Liquid on a Convectively Cooled Wall. Proceedings of the Third International Heat Transfer Conference, Chicago, ASME, AIChE, Aug. 1966, vol. IV, pp. 141-151.

23. Johnson, Victor J.: A Compendium of the Properties of Materials at Low Temperatures. Part 2. Properties of Solids. (WADD TR 60-56, pt. 2), National Bureau of Standards, Cryogenic Eng. Lab., Oct. 1960.

24. Tebo, F. J.: Selected Values of the Physical Properties of Various Materials. Rep. No. ANL-5914, Argonne National Lab., Sept. 1958.

25. Ratcliffe, E. H.: The Thermal Conductivity of Ice-New Data on the Temperature Coefficient. Philosophical Mag., vol. 7, no. 79, July 1962, pp. 1197-1203.

26. Powell, R. W.: Preliminary Measurements of the Thermal Conductivity and Expansion of Ice. Roy. Soc. Proc., vol. 247, no. 1251, Oct. 21, 1958, pp. 464-466.

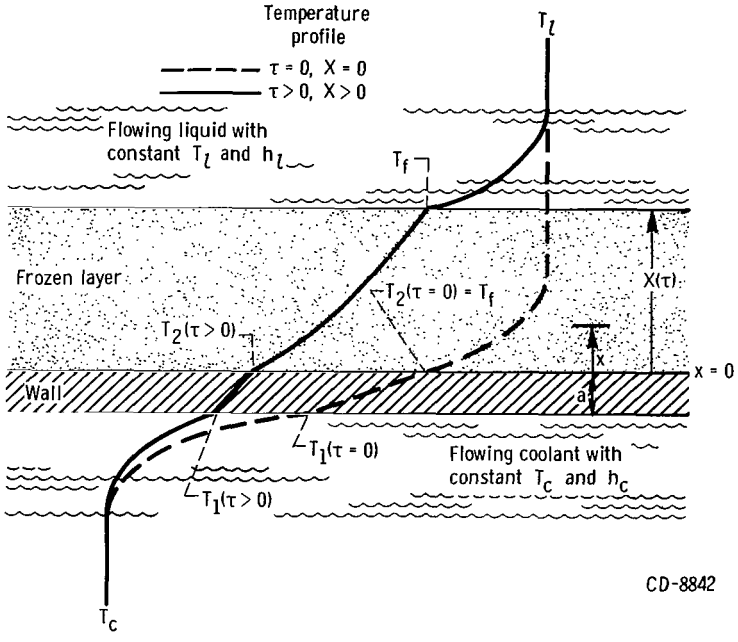

Figure 1. - One-dimensional model of transient solidification in warm liquid flowing over convectively cooled plate.

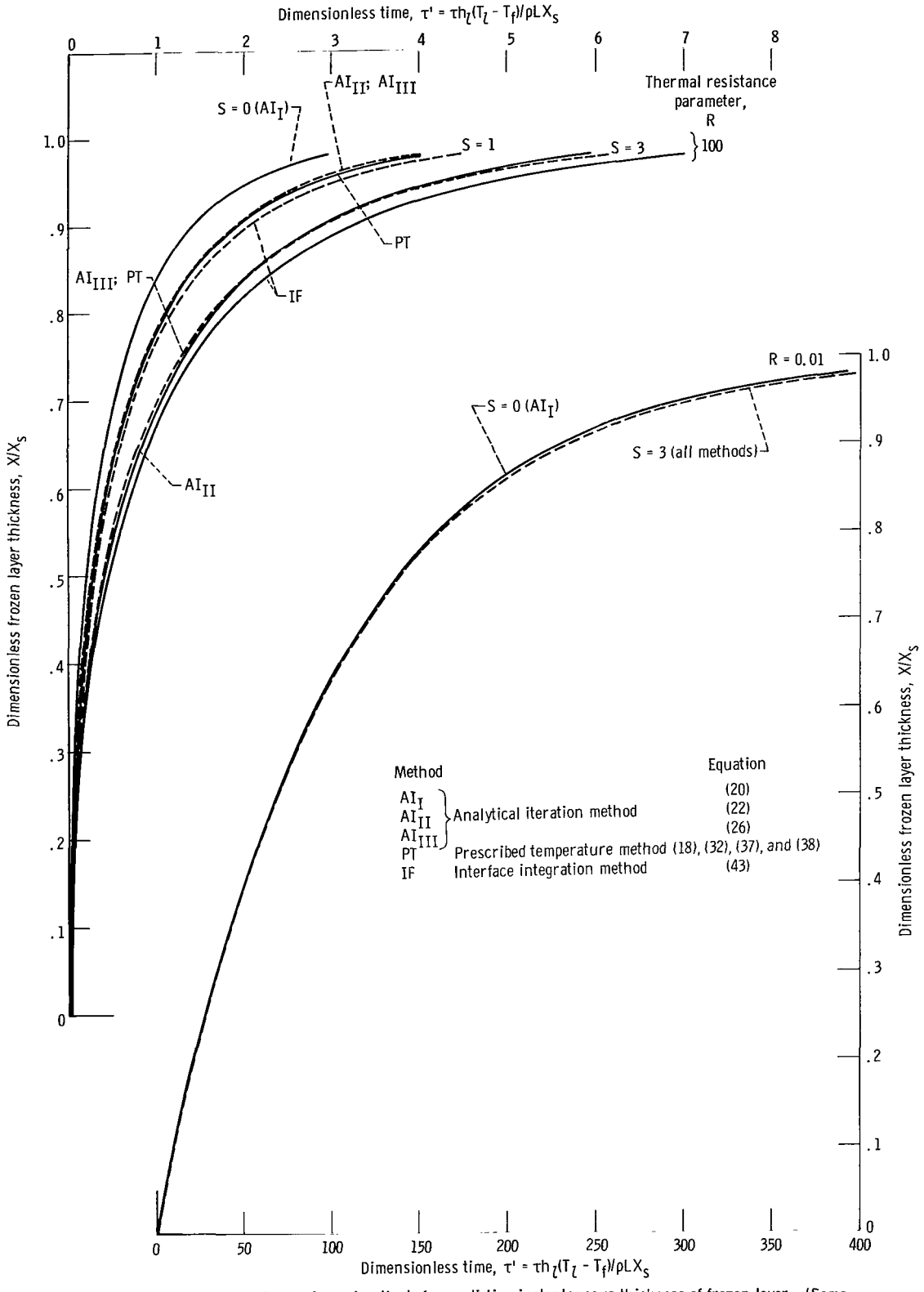

Figure 2. - Comparison of methods for predicting instantaneous thickness of frozen layer. (Some curves dashed for clarity only.)

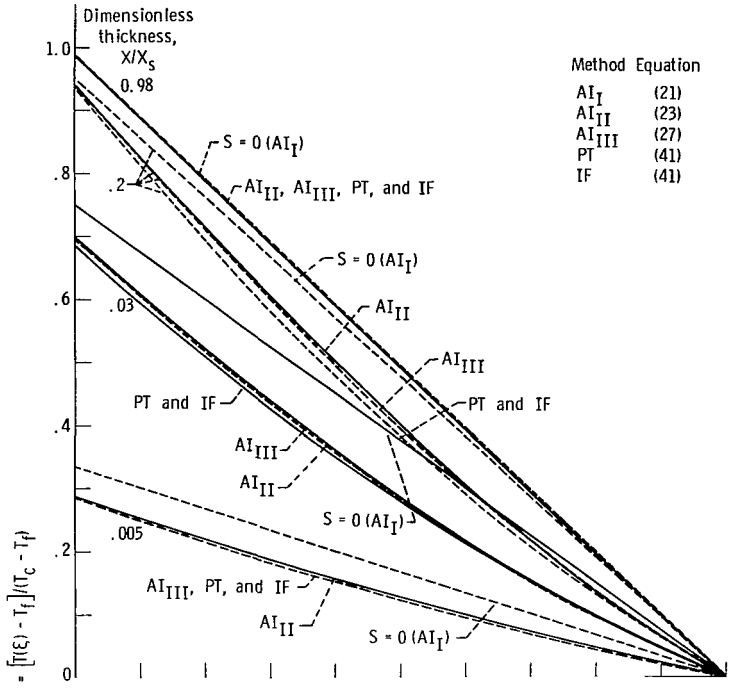

(a) Thermal resistance parameter, R = 100; subcooling parameter, S = 3.

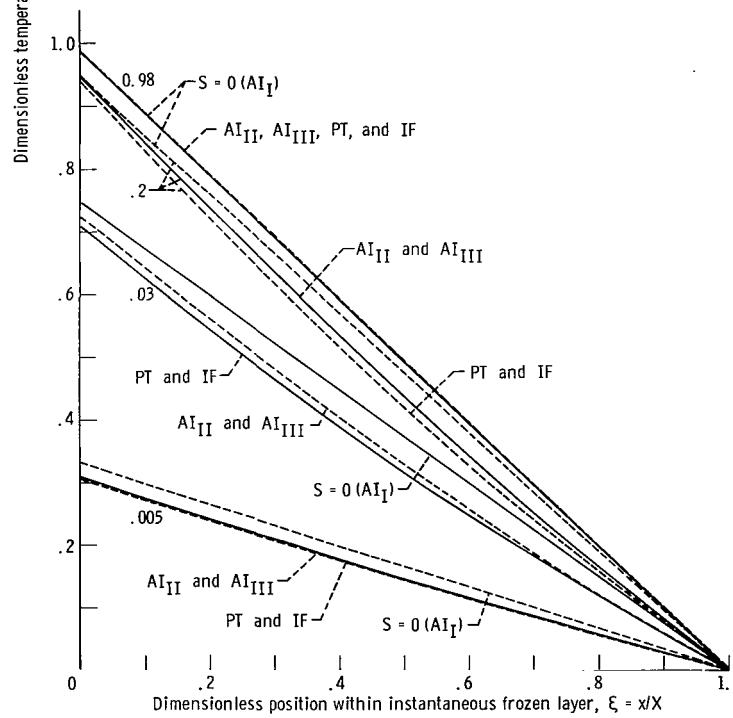

(b) Thermal resistance parameter, R = 100; subcooling parameter, S = 1.

Figure 3. - Temperature distributions in frozen layer computed by various methods. (Some curves dashed for clarity only.)

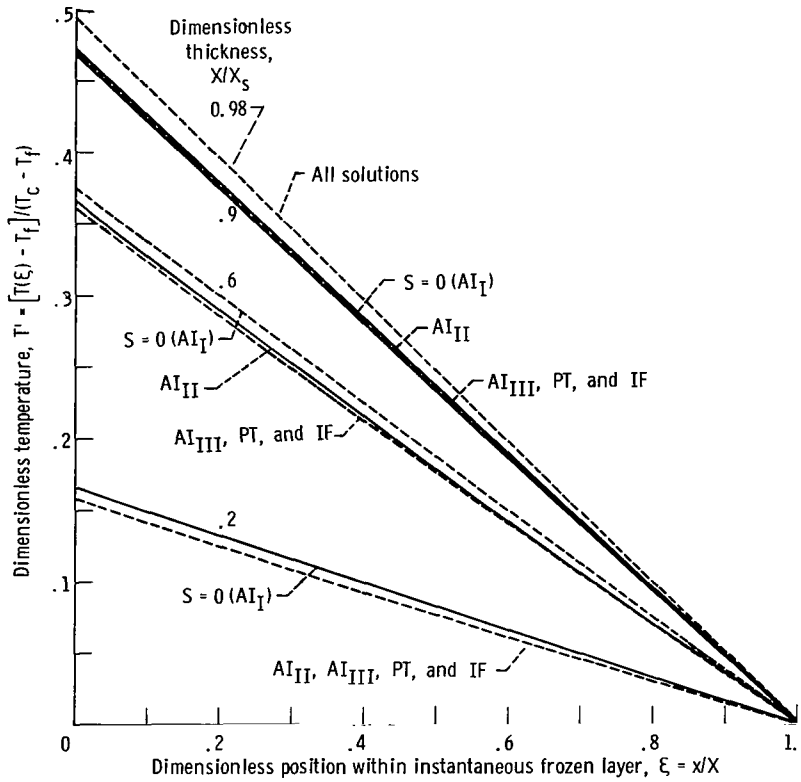

(c) Thermal resistance parameter, R = 1; subcooling parameter, S = 3.

Figure 3. - Concluded.

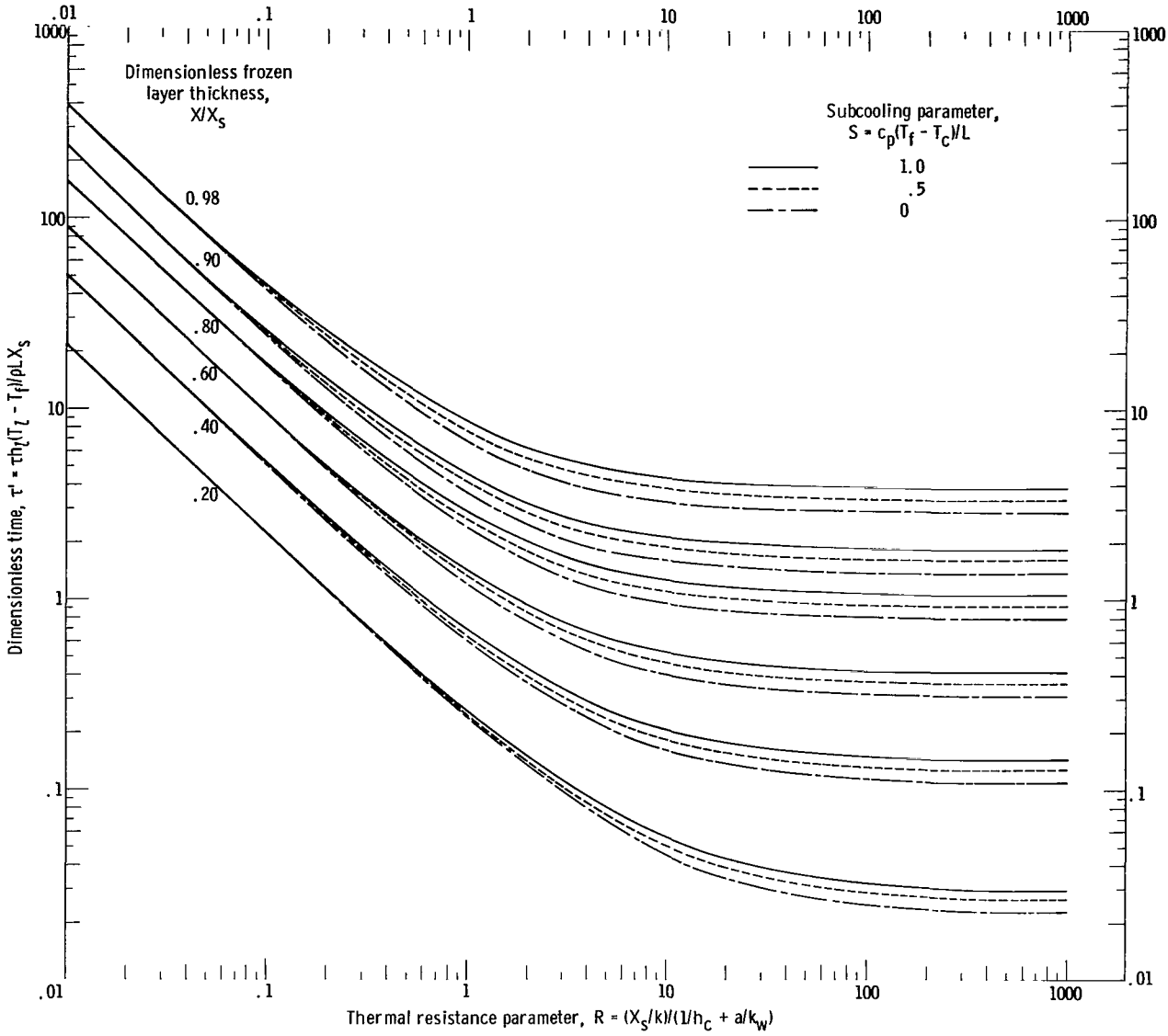

(a) Subcooling parameters, 0, 0.5, and 1.

Figure 4. - Dimensionless growth times as function of thermal resistance parameter for various dimensionless thicknesses and subcooling parameters.

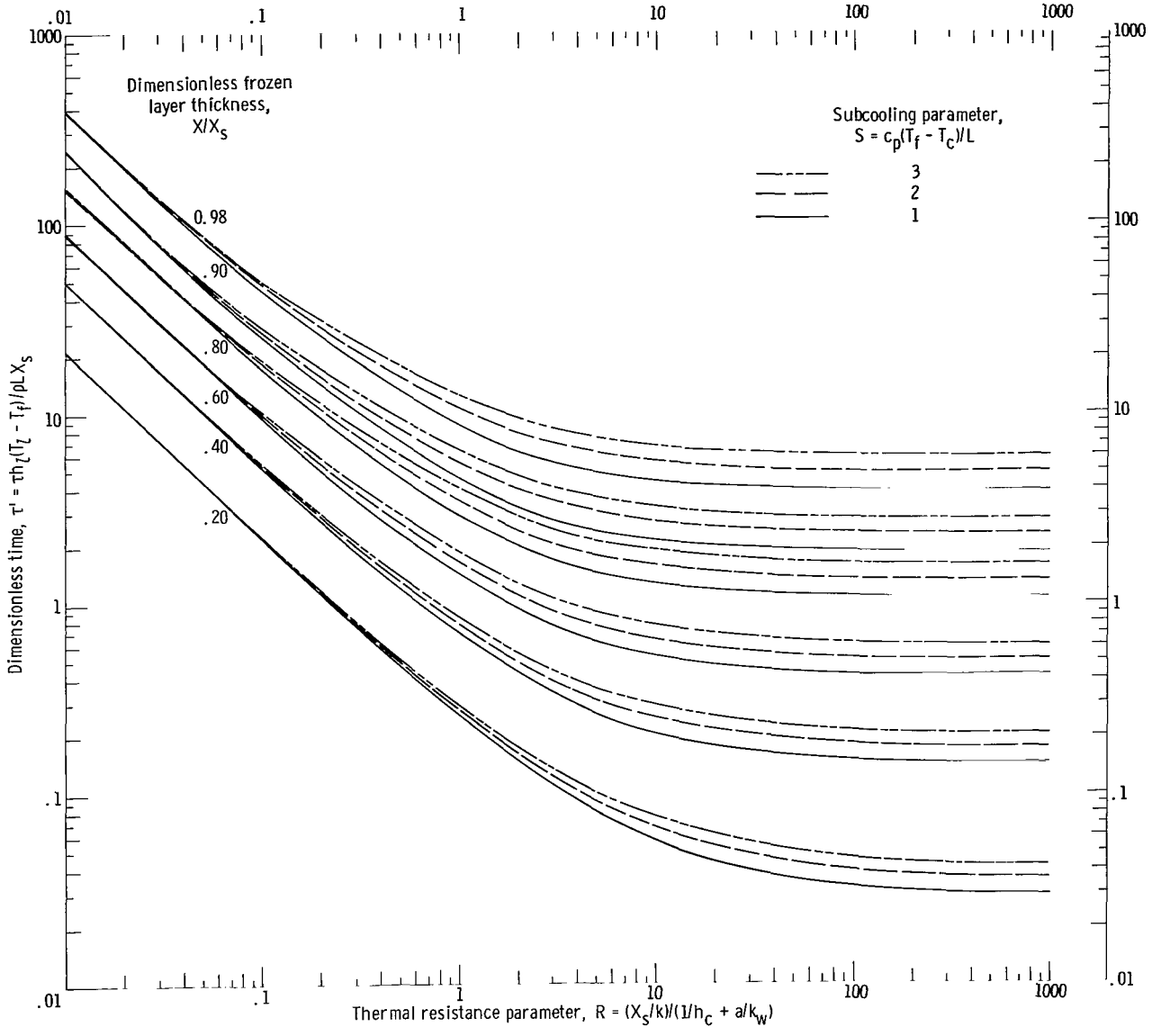

(b) Subcooling parameters, 1, 2, and 3.

Figure 4. - Concluded.

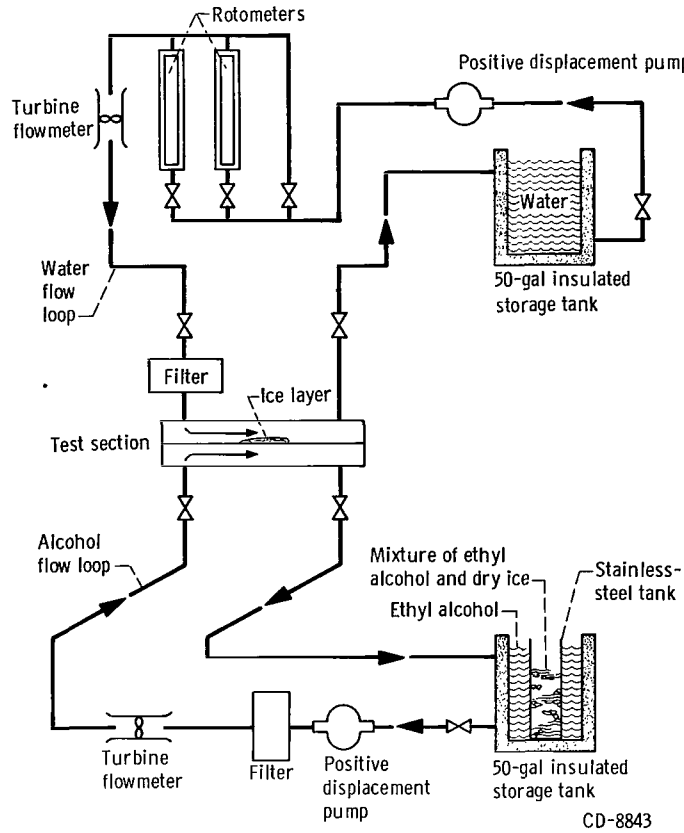

(a) Water and alcohol flow circuits.

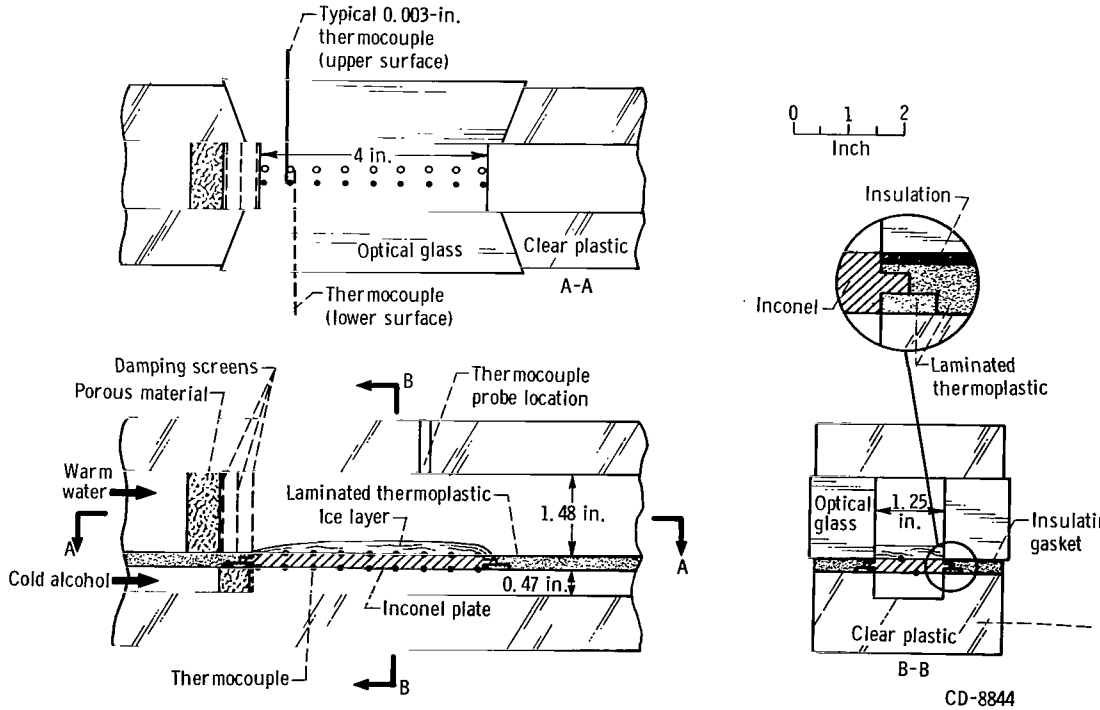

(b) Details of test section.

Figure 5. - Test apparatus.

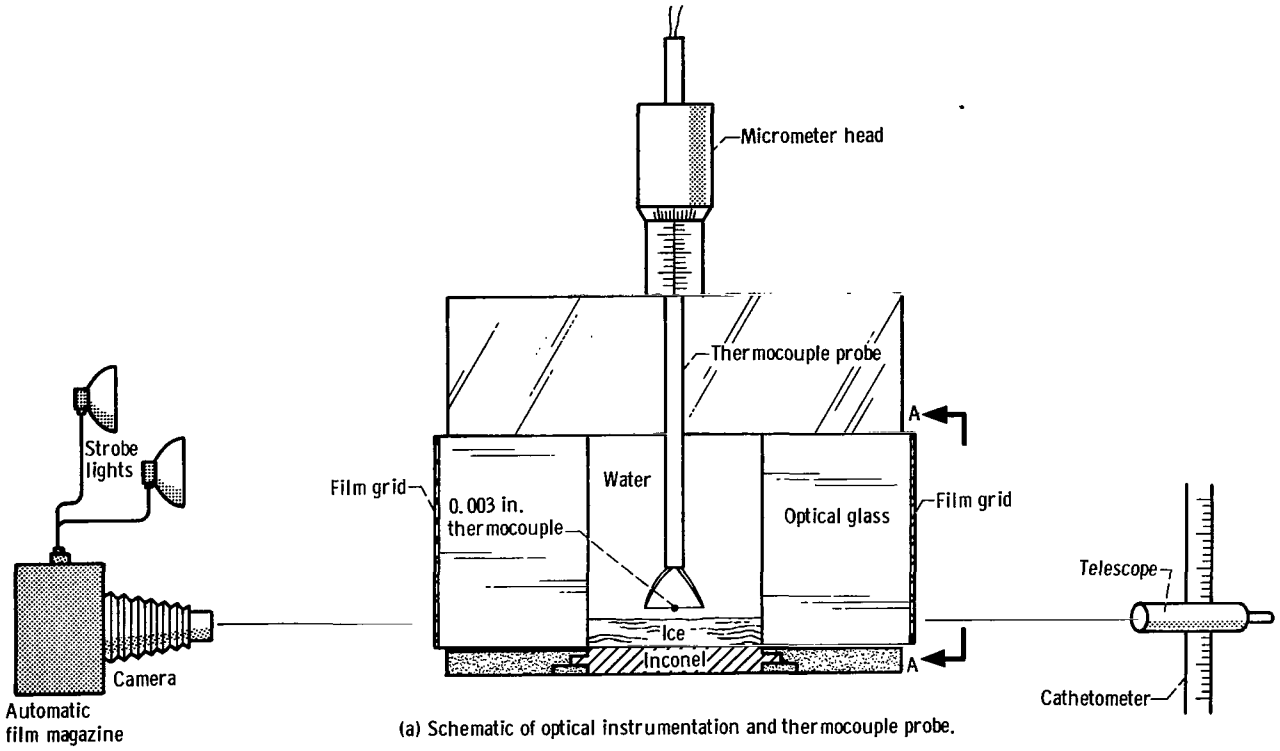

(a) Schematic of optical instrumentation and thermocouple probe.

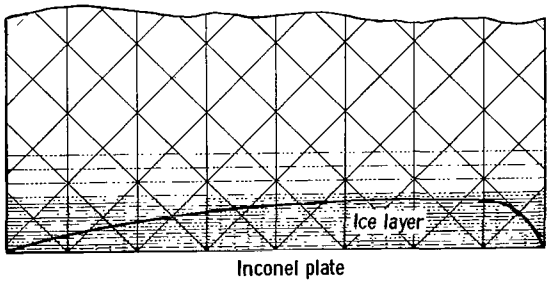

8845-S

(b) Schematic of film grid.

Figure 6. - Devices for measuring ice thickness.

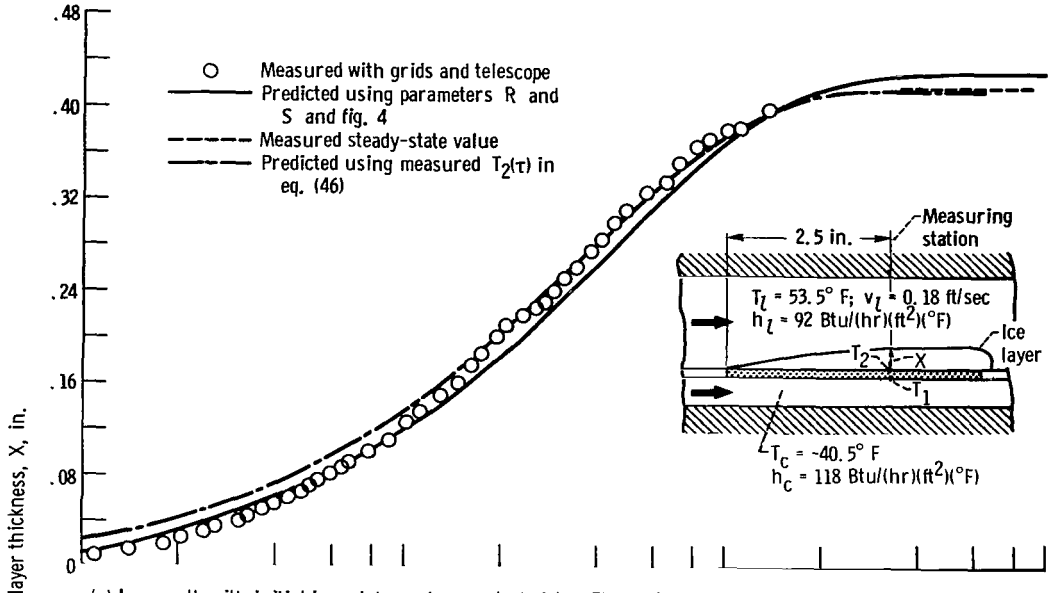

(a) Ice growth with initial ice patch nucleus on test plate. Thermal resistance parameter, R = 2.55; subcooling parameter, S = 0.232.

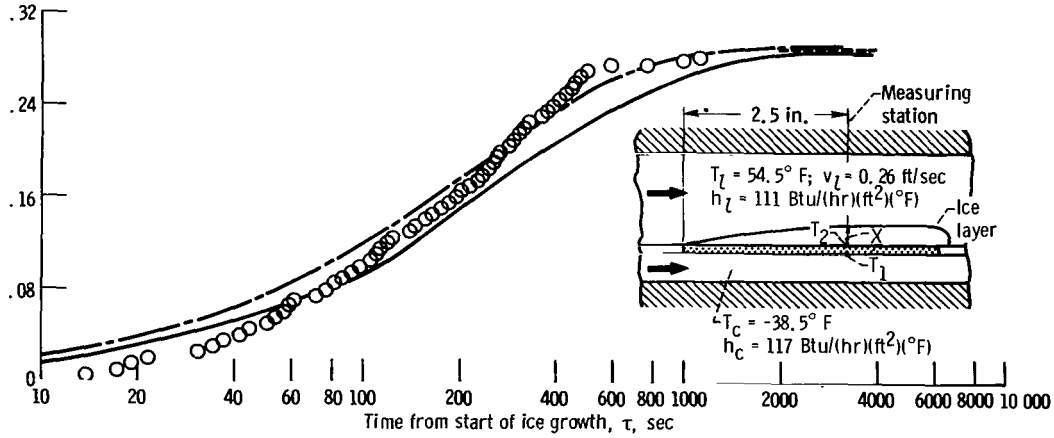

(b) Ice growth with initial ice patch nucleus on test plate. Thermal resistance parameter, R = 1.67; subcooling parameter, S = 0.225.

Figure 7. - Comparison of measured with theoretically predicted ice thicknesses. (Plate temperature transients are in corresponding parts of fig. 8).

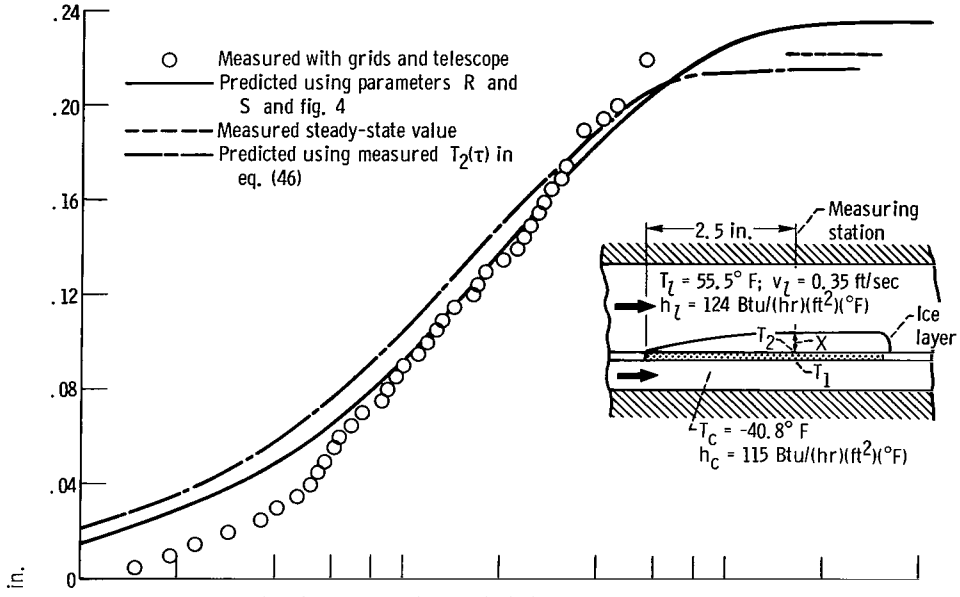

(c) Ice growth with initial ice patch nucleus on test plate. Thermal resistance parameter, R = 1.35; subcooling parameter, S = 0.232.

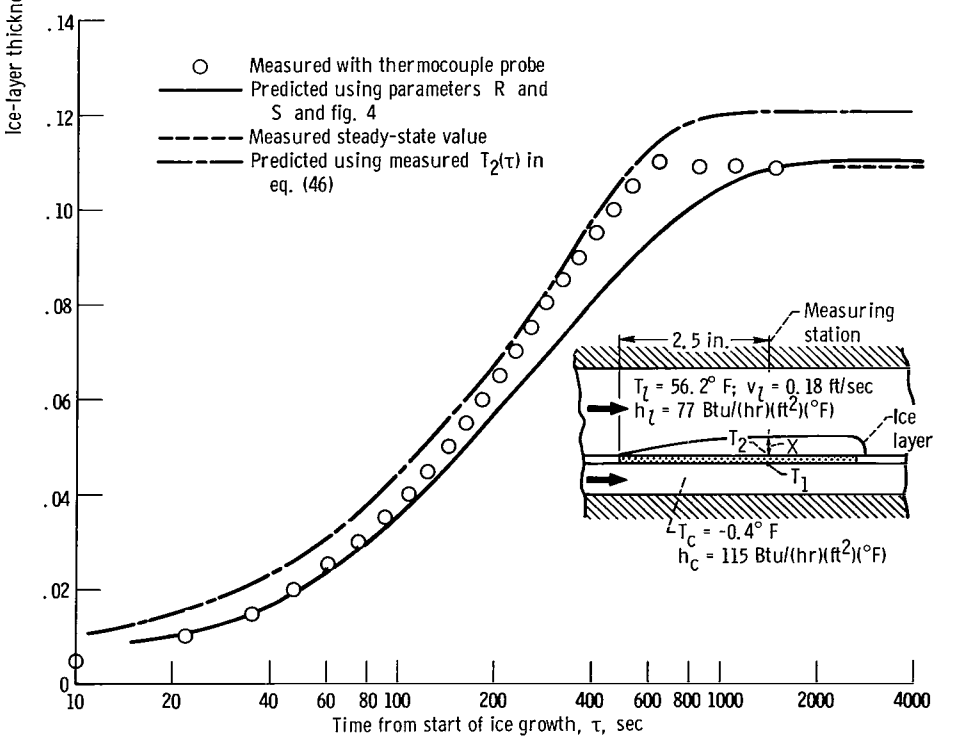

(d) Ice growth with initial ice patch nucleus on test plate. Thermal resistance parameter, R = 0.631; subcooling parameter, S = 0.104.

Figure 7. - Continued.

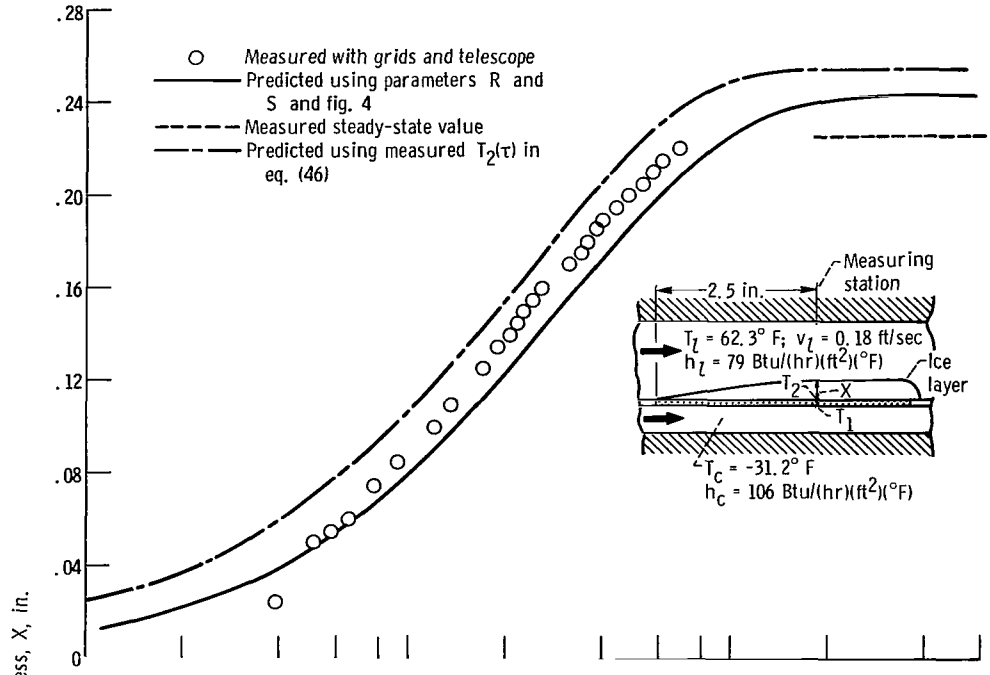

(e) Ice growth without initial ice patch nucleus on test plate. Thermal resistance parameter, R = 1.21; subcooling parameter, S = 0.202.

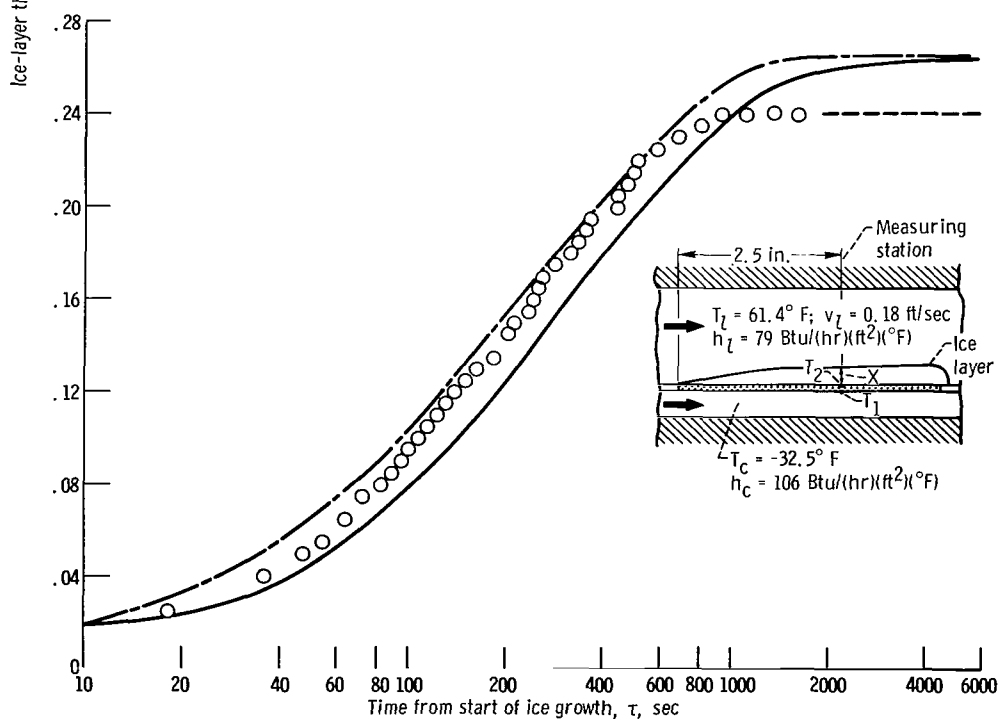

(f) Ice growth with initial ice patch nucleus on test plate. Thermal resistance parameter, R = 1.29; subcooling parameter, S = 0.206.

Figure 7. - Concluded.

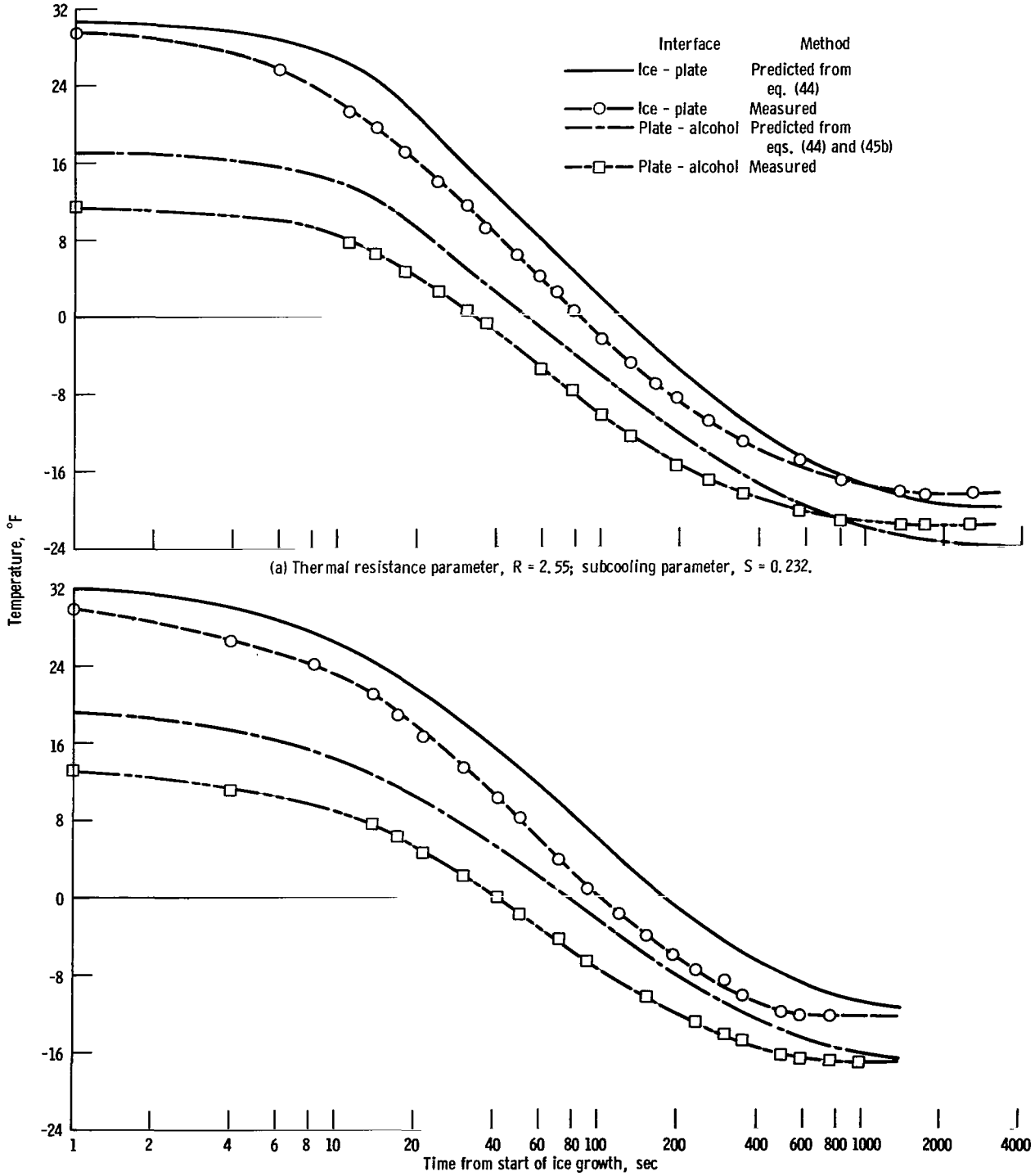

(a) Thermal resistance parameter, R = 2.55; subcooling parameter, S = 0.232.

(b) Thermal resistance parameter, R = 1.67; subcooling parameter, S = 0.225.

Figure 8. - Temperature transients of test plate surfaces. (Each part of fig. 8 corresponds to same part of fig. 7.)

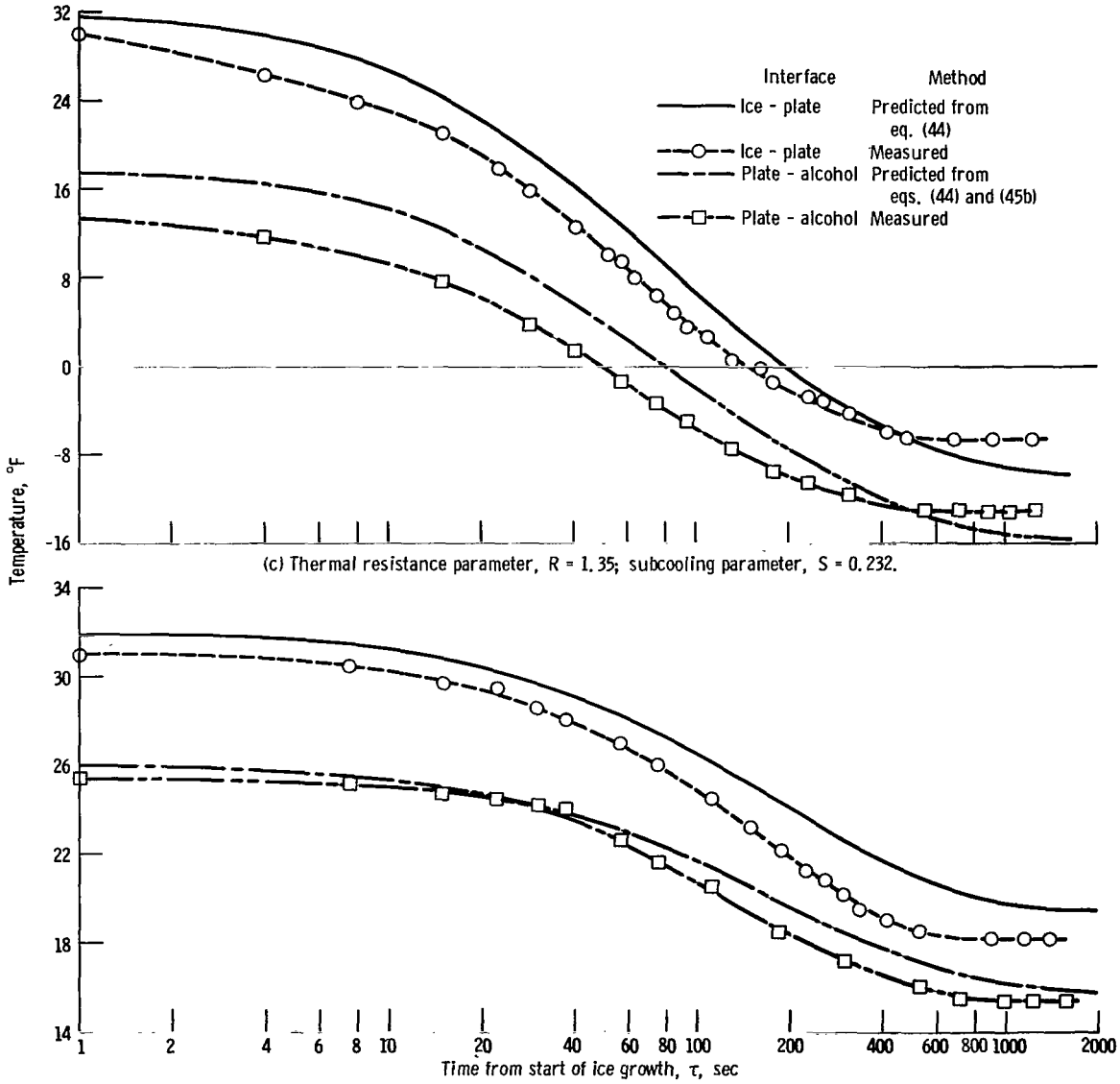

(c) Thermal resistance parameter, R = 1.35; subcooling parameter, S = 0.232.

(d) Thermal resistance parameter, R = 0.631; subcooling parameter, S = 0.104.

Figure 8. - Continued.

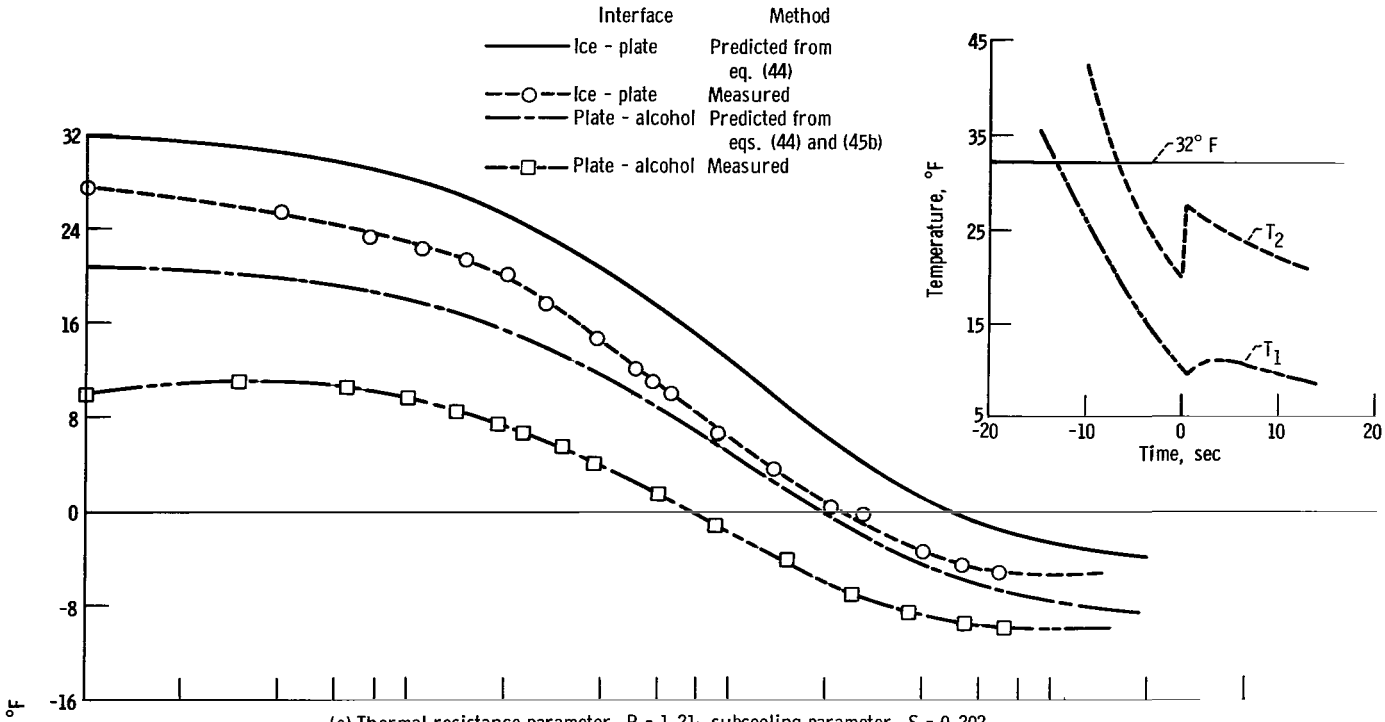

(e) Thermal resistance parameter, R = 1.21; subcooling parameter, S = 0.202.

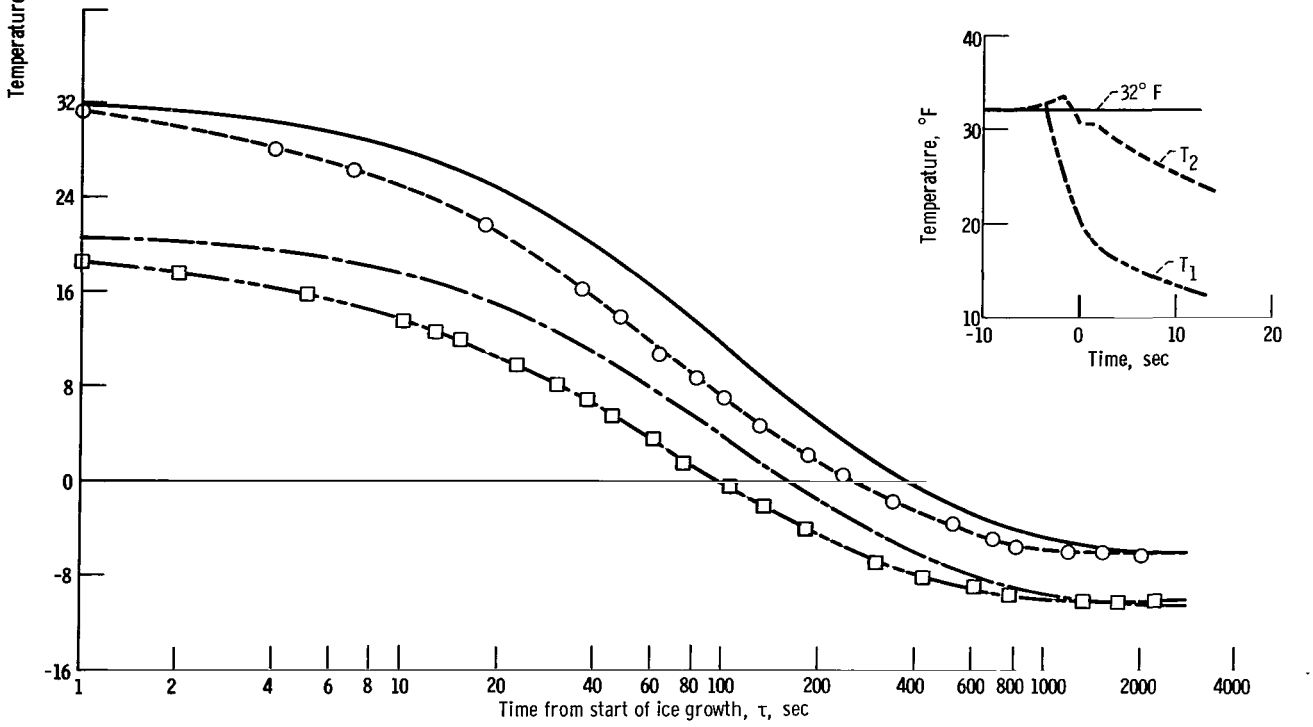

(f) Thermal resistance parameter, R = 1.29; subcooling parameter, S = 0.206.

Figure 8. - Concluded.

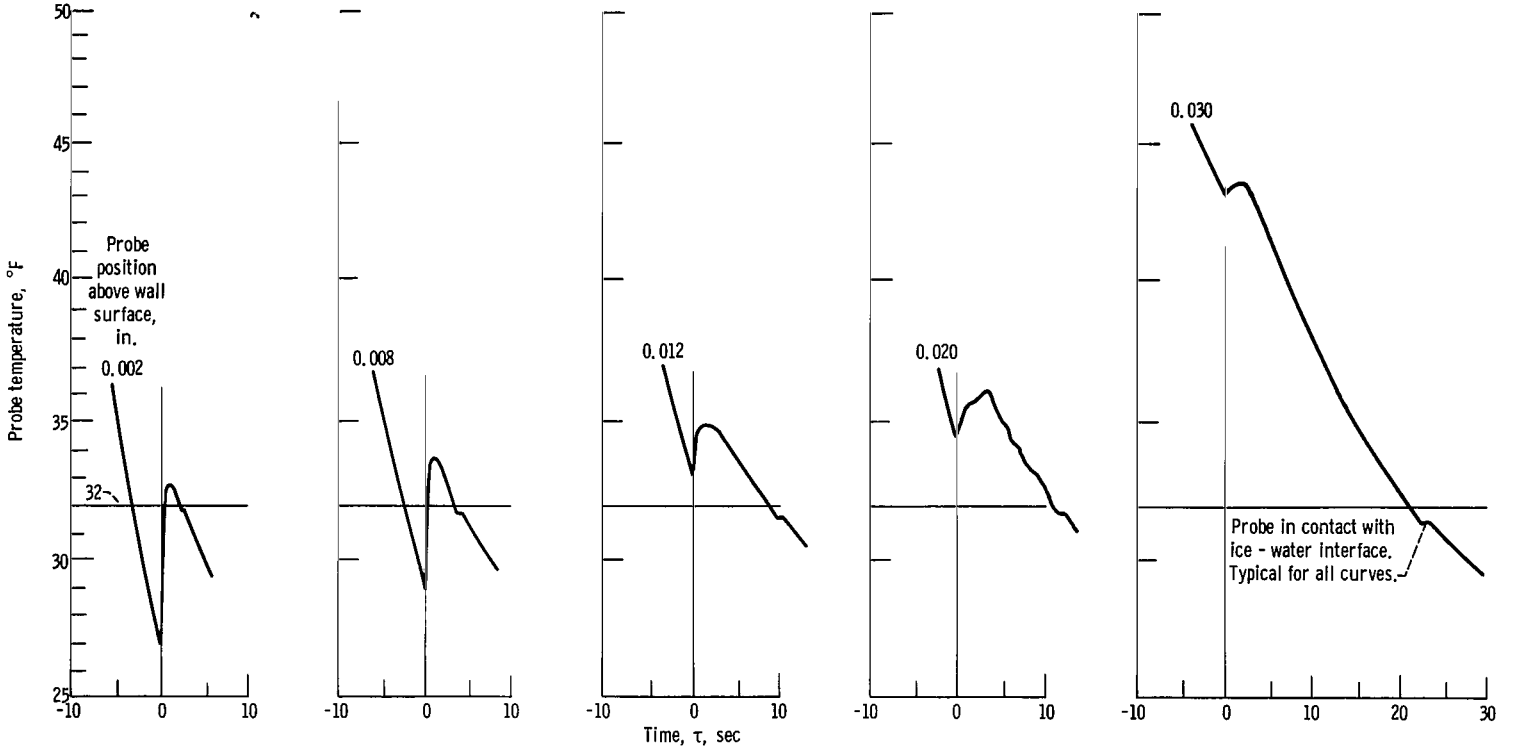

(a) Temperature-time history measured by probe at various fixed positions above plate surface.

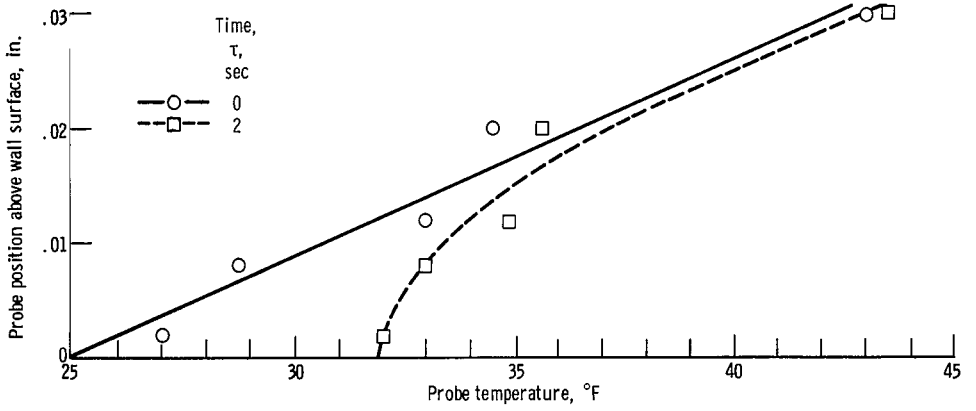

(b) Temperature profile in water thermal boundary layer an instant before nucleation and 2 seconds later.

Figure 9. - Temperature behavior in water thermal boundary layer before and after spontaneous ice nucleation on a subcooled plate.

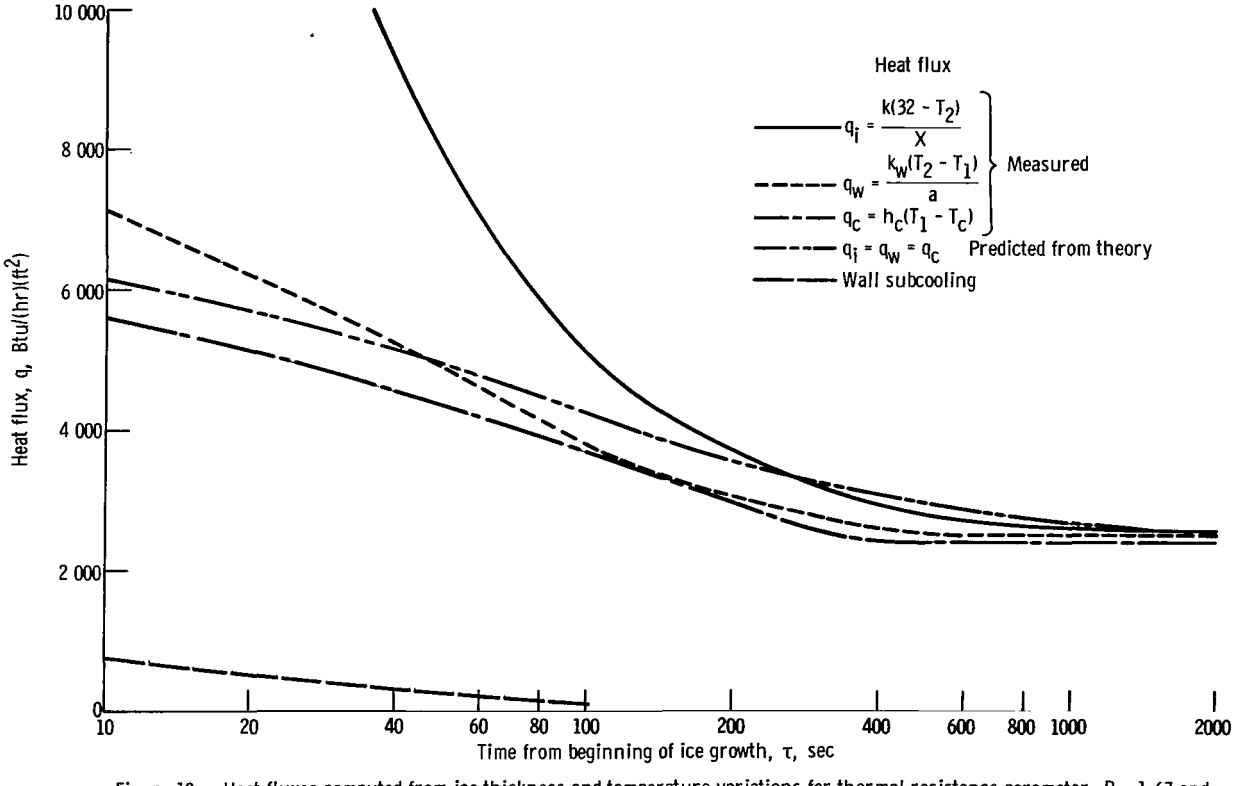

Figure 10. - Heat fluxes computed from ice thickness and temperature variations for thermal resistance parameter, R = 1.67 and subcooling parameter, S = 0.225.

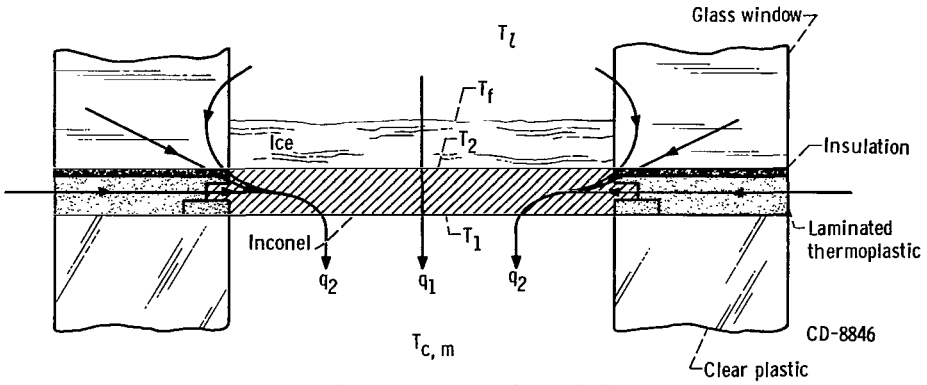

Figure 11. - Paths for heat leakage into coolant.

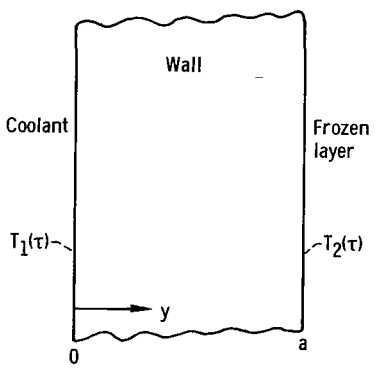

Figure 12. - Coordinate system in wall.

"The aeronautical and space activities of the United States shall be conducted so as to contribute . . . to the expansion of human knowledge of phenomena in the atmosphere and space. The Administration shall provide for the widest practicable and appropriate dissemination of information concerning its activities and the results thereof."

—NATIONAL AERONAUTICS AND SPACE ACT OF 1958

NASA SCIENTIFIC AND TECHNICAL PUBLICATIONS

TECHNICAL REPORTS: Scientific and technical information considered important, complete, and a lasting contribution to existing knowledge.

TECHNICAL NOTES: Information less broad in scope but nevertheless of importance as a contribution to existing knowledge.

TECHNICAL MEMORANDUMS: Information receiving limited distribution because of preliminary data, security classification, or other reasons.

CONTRACTOR REPORTS: Scientific and technical information generated under a NASA contract or grant and considered an important contribution to existing knowledge.

TECHNICAL TRANSLATIONS: Information published in a foreign language considered to merit NASA distribution in English.

SPECIAL PUBLICATIONS: Information derived from or of value to NASA activities. Publications include conference proceedings, monographs, data compilations, handbooks, sourcebooks, and special bibliographies.

TECHNOLOGY UTILIZATION PUBLICATIONS: Information on technology used by NASA that may be of particular interest in commercial and other non-aerospace applications. Publications include Tech Briefs, Technology Utilization Reports and Notes, and Technology Surveys.

Details on the availability of these publications may be obtained from:

SCIENTIFIC AND TECHNICAL INFORMATION DIVISION

NATIONAL AERONAUTICS AND SPACE ADMINISTRATION

Washington, D.C. 20546